NASA CONTRACTOR REPORT

NASA CR-1472

EFFECT OF JET TEMPERATURE ON JET AND PURE TONE NOISE RADIATION

by Harry E. Plumblee, George A. Wynne, and Ben T. Zinn

Prepared by
LOCKHEED-GEORGIA COMPANY
Marietta, Ga.
for Langley Research Center

NATIONAL AERONAUTICS AND SPACE ADMINISTRATION • WASHINGTON, D. C. • NOVEMBER 1969

EFFECT OF JET TEMPERATURE ON JET AND PURE TONE NOISE RADIATION

By Harry E. Plumblee, George A. Wynne, and Ben T. Zinn

Prepared under Contract No. NAS 1-8443 by
LOCKHEED-GEORGIA COMPANY
Marietta, Ga.

for Langley Research Center

NATIONAL AERONAUTICS AND SPACE ADMINISTRATION

For sale by the Clearinghouse for Federal Scientific and Technical Information
Springfield, Virginia 22151 – Price $3.00

CONTENTS

EFFECT OF JET TEMPERATURE ON JET AND PURE TONE NOISE RADIATION

By

Harry E. Plumblee
George A. Wynne
Ben T. Zinn*

Lockheed-Georgia Company

SUMMARY

A model jet nozzle was tested over a temperature range of 540°R to 1100°R, and sound pressure was measured at enough positions in the far field to calculate sound power. From these tests, the effect of temperature on total sound power was isolated. A prediction technique for sound pressure, developed from an earlier test program, was modified to sound power and was verified over the temperature test range of this program. The prediction method was then used to determine the effect of temperature, as high as 3500°R, on radiated sound power. It was determined that jet sound power is a non-linear function of temperature and that, at high temperatures, significant reductions in jet noise may be achieved.

Tests were also run to ascertain the changes in fan noise characteristics as the noise propagates through a high-temperature region in the fan duct and subsequently radiates into an ambient medium. Although the test results were rather inconclusive, it was shown that increasing temperature increases higher-order acoustic duct mode cut-on frequencies, and that increasing temperature possibly reduces radiated pure tone noise.

Design studies were made concerning the changes required to modify an existing engine to test the jet-heating concept. These studies dealt with duct combustion chamber geometry, flameholder aerodynamics, fuel injection and ignition, and burning and heat transfer.

Because of the possibility that a duct burner will exhibit combustion instabilities and since basically acoustic nature of the proposed tests precludes the use of an acoustic liner, a combustion instability analysis for annular duct geometry was performed. The analysis was used as a guide in designing components such as the combustion chamber and flameholders, to reduce the probability of experiencing high frequency combustion instability.

---

* Associate Professor, School of Aerospace Engineering, Georgia Institute of Technology. Consultant to the Lockheed-Georgia Company.

INTRODUCTION

The decision of Congress to provide the FAA the governing power to impose restrictions on radiated noise of aircraft during takeoff and approach stages of flight has touched off a flood of research and development efforts directed toward the problem of reducing aircraft engine radiated noise levels. Of course, due to the nature of the noise source from existing and future bypass fan engines, most of the research has been directed toward finding a method of reducing fan-blade-generated periodic-tone noise. However, workers continue the search for optimized methods to reduce jet noise as well.

It has been well established that aircraft turbofan and turbojet engines present two distinct noise-generating mechanisms. The highly random broad-band noise which has now become characteristic of a jet flow received the most prominent first attention. Research into methods of reducing jet flow noise began 20 years ago, and three basic methods for reducing jet noise were formulated. These involved changing the basic jet directivity, changing the jet mixing process, or reducing the jet velocity. Methods for changing the mixing were used quite extensively on commercial turbojets in the form of multilobe nozzles.

It gradually became evident, however, that the real potential for reducing jet noise lay in the approach of reducing jet velocity. This great potential (it is well established that sound power is proportional to jet velocity raised to the 6th or 8th power) was finally achieved as a favorable byproduct in the development of an entirely new type of power-plant: the turbofan engine. However, the new noise problems introduced by this engine were just as severe as those of the jet engine but of a different nature. Now, a new generation turbofan engine has been introduced - the high bypass ratio turbofan. The more promising commercial versions have been designed for low noise. They effect removal of inlet guide vanes, provide separate speeds for the turbine and compressor stages, and have the outlet guide vanes or struts highly separated from the rotor stage.

However, in spite of these considerable technical improvements, it is still necessary to reduce the noise radiated from advanced-technology turbofan engines. The objectional noise is that generated by the compressor blades (and sometimes the turbine stage) rather than the jet noise. So far, the best method of reducing this fan-generated noise is offered by the optimum application of sound-attenuating liner materials to the interior of the engine inlet and exhaust ducting. However, this technique involves serious practical problems. One of the new-generation transports in the 3/4-million-pound class may require as much as 10,000 pounds of additional weight to accomplish the required noise reduction. Furthermore, fuel consumption will probably increase as a result of increased internal drag in the engine nacelle. Therefore, although creative engineering and scientific efforts have responded to the demand to reduce aircraft noise, improved methods would be widely welcomed.

A field for research which has received little attention is the effect of jet density on engine noise. This study deals with temperature change, the most promising method available for controlling jet density in an air-breathing, subsonic engine. Primarily, the work was intended as a feasibility study; since the acoustic effects attributed to temperature at the time this research was proposed were based on previous work, but mainly were in the form of hypotheses. Also, many problems were anticipated if the concepts were to be applied either to an existing engine or to a model fan/burner system built solely to demonstrate the acoustic effects described. Therefore, this research program was directed toward crystalizing the temperature effects on radiated noise and determining the major problems anticipated in demonstrating the effects in a realistic situation.

Experimental acoustic data were obtained on the effects of jet temperature on radiated noise, both jet noise and simulated fan-blade noise.

Since the use of high exhaust temperature in a turbofan would demand a major modification, if applied to an existing engine, work was also done to determine the requirements to introduce heating into a fan engine duct, and research was conducted on one of the major problems anticipated: combustion instability. The results described in the Appendix cover the problems one would expect to encounter in modifying an existing engine or in building a model to verify temperature effects on noise.

Much of the work in reducing, correlating and analyzing the jet noise data used in this report was done by G. P. Haddle (refs. 1 and 2). Some of the work in Appendix A on ignition and combustion was done by M. D. Bowen.* The authors gratefully acknowledge these substantial contributions.

SYMBOLS

A	exhaust area
c	speed of sound
C_p	specific heat at constant pressure
h	ratio of the number of water-vapor molecules to the total number of molecules per unit volume of the atmosphere
I	sound intensity
J_m, N_m	Bessel and Neumann functions of m^{th} order
k	wave vector
L	Lighthill parameter
M	Mach number
$\overline{P}$	root-mean-square sound pressure
P	sound power
P_N	normalized sound power
r	distance from source location to field point, non-dimensionalized to nozzle exit diameter
S	area used to calculate sound power from sound pressure
T	total temperature - ^oR

*Senior Research Engineer & Lecturer, School of Mechanical Engineering, Georgia Institute of Technology. Consultant to the Lockheed-Georgia Company.

T_j	exit static temperature - $^\circ R$
V	exit plane velocity
z	distance (used in eq (2))
γ	ratio of specific heats - also wave propagation vector in eq. 10.
δ	diffusivity of sound (as defined in reference 5)
θ	angle from field point to jet thrust axis, referenced to nozzle exit plane
μ	coefficient of shear viscosity
μ'	effective bulk viscosity
ρ_j	jet density (static)
ρ_o	atmospheric density
T	thrust
ω	radial frequency

TEMPERATURE EFFECTS ON AIRCRAFT ENGINE NOISE

The original conception of this research was that it would be a complete study of the effect of temperature (only as an effect on density) on radiated jet noise. The objective was to determine if jet noise reduction could be achieved by heating the bypass air of a turbofan engine. As a means of implementing the objective, a very complete noise survey was made for a number of model jet nozzles where temperature and nozzle size were varied. Enough tests were conducted to isolate the effect of velocity (which, of course, has already been well established in a number of experiments and analyses), nozzle size and temperature (or density). The result of these tests was presented by Haddle and Plumblee (ref. 1), and a complete data report was published by Haddle, Wynne and Mathis (ref. 2).

It was also observed, that if the turbofan bypass air were heated by an afterburner method, aft-radiated fan noise must refract from a nearly atmospheric-density region behind the fan blades to a very low-density region aft of the burning stage. Subsequently, the noise refracts back to atmospheric conditions through the jet mixing boundary. This multiple reflection-refraction process was certain to affect the directivity of the fan-generated noise and would probably affect the level of radiated noise. To try to determine the effects of jet heating on turbofan noise, a series of tests was run which simulated the actual engine conditions to some extent. In these tests, a pure tone sound pressure distribution was injected from an ambient medium, through the hot air jet, and allowed to radiate into an ambient atmosphere anechoic room. From these series of tests, an order of magnitude effect of the hot air could be ascertained. The effects of temperature on both jet noise and fan noise is discussed below.

Temperature Effects on Jet Noise

The effect of density on jet noise was first investigated in 1952 by Lassiter and Hubbard (ref. 3). In their study, a series of tests was conducted with helium, freon and air jets. Noise was measured on a circle around the jet and was reported in detail for a point in the far field 90° from the jet axis. The results of their experiment showed that overall sound pressure was directly proportional to jet density at that position in the radiated noise field. It is believed that this set of experiments led to the modified form of Lighthill's relationship for jet power which was commonly used in jet noise prediction methods. The modification was of the form

$$\text{sound power} \propto \frac{\rho_j^2}{\rho_o^2} L$$

where L is the Lighthill parameter, $\frac{\rho_o A V^8}{C_o^5}$

The authors of the reference 3 study did not suggest that sound power would follow the same trends as sound pressure. This would, of course, presuppose that changes in jet density would not affect directivity. It is now well known that jet density does affect directivity, and the Lassiter and Hubbard report also documented the directivity effect in figure 9 of reference 3. This directivity plot showed that, for the cold air jets, the peak in radiated overall sound occurred at an angle of 15° from the jet axis, while the helium jet noise peaked at 40° to 45°. The jets were operated at the same exit Mach number.

In a later study (ref. 4) it was shown that, for a series of tests with subsonic and supersonic heated jets, the far-field sound pressure 90° from the jet axis was proportional to jet density raised to the 0.8 power. These tests were run over a broad range of parameters; velocity was varied from 900 ft/sec to nearly 4000 ft/sec, and exhaust static temperature was varied from ambient to 2800°R. Therefore, $\rho^{0.8}$ was derived from quite a large range of jet parameters. However, since half of the tests were conducted at supersonic exhaust velocities, it might be argued that the high Mach numbers would significantly affect the trends. But, on closer examination of the data in reference 4, it was determined that the trends were more or less uniform over the complete test range. The region where the velocity law changes from 8th power to 3rd power occurs at an eddy convection Mach number of 1. Since the eddy convection Mach number is roughly one-half the jet Mach number, the tests conducted in reference 4 did not have an eddy convection Mach number which exceeded 1, and it would be expected that the effects of Mach number would be uniform over the test range.

Description of test program.- Since the objective was to determine the effect of temperature on radiated sound pressure level at constant thrust and velocity, the ideal way to conduct the test would be to design a series of nozzles of different sizes to be tested at one velocity, which would all have the same thrust if tested at the design temperature and velocity. However, a more practical test, which would yield considerably more useful information, would use the same series of nozzles in a complete parameter variation of temperature and velocity. Four conical nozzles were designed and were operated at the test conditions listed in table I. Several repeat runs were made for selected nozzles.

A schematic diagram of the hot-air generation and control system is shown in figure 1. The burner system used operates on propane, and all products from combustion remain in the

hot air. During the time required to bring the system up to a given temperature/pressure condition at the nozzle, the room was continuously cooled with a bypass air supply. Once a test condition was reached, the cooling air was rapidly closed down, and then noise data were recorded. As soon as a set of noise data was successfully recorded, the cooling air was once again applied. This, of course, was required to prevent the hot air supply from burning up the interior of the anechoic room and damaging the instrumentation.

The data recording and calibration system is schematically represented in figure 2, while the data analysis system for determining 1/3 octave spectra and total power level is given in figure 3. A calibrated sound pressure level was introduced into each microphone and recorded on the magnetic tape so that absolute SPL could easily be determined. The data were recorded at a tape speed of 60 inches per second. Then, during data reduction, the tape playback speed was 7.5 inches per second. At playback, the data were passed through an octave band analyzer, and center frequencies of 63 Hz to 8 KHz were used. This corresponds to a bandwidth of 300 Hz to 80 KHz for the actual data analysis.

Acoustic power calculation.- The total radiated acoustic power was calculated by summing the power attributed to each microphone.

$$P = \sum_i I_i S_i = \sum_i \frac{\overline{P}_i S_i}{\rho c} \tag{1}$$

where it is assumed that the intensity at the i^{th} station is $\overline{P}_i/\rho c$.

This calculation was accomplished with a digital computer for overall power levels and eight octave bands. The area allocated to each microphone is illustrated in figure 4. The data from microphone 1 were eliminated in the final power calculation because of severe buffet signals which appeared on the microphone output. This microphone would not contribute significantly to the total acoustic power because the sound pressure is relatively low at station 1 and the area allocated to station 1 is small in comparison to the total area.

Effect of velocity on total acoustic power.- Before trying to ascertain the effect of temperature, it was necessary to establish what velocity law the model jet was following, since the 8^{th} power law is not always found in practice. For instance, in reference 4, something closer to a 6^{th} power law was experimentally determined. Also, reference 3 reported a 6^{th} power law for a full-scale turbojet. Figures 5 and 6 are plots of the sound power level, showing the functional relationship with exit velocity for all four nozzles and two different exit static temperatures. The solid lines plotted through the data are proportional to 8^{th} power law. From examination of the data in these two charts, it is certainly justifiable to specify an 8^{th} power velocity law for the tests in this analysis.

The 8^{th} power trend lines for each nozzle are separated by 10 log A_n/A_4, where A_n/A_4 is the ratio of nozzle area referenced to the largest nozzle area. It is observed that all the data are fairly accurately separated by the nozzle area ratio, except for the smallest nozzle. It was hypothesized that, since the noise spectrum from the smaller nozzle peaked at a higher frequency, high-frequency atmospheric attenuation could be reducing the spectrum peak. However, if the method attributed to Lighthill in reference 5 is used, very small attenuations are calculated, even at the highest frequency used in the frequency analysis of the jet noise.

Briefly, Lighthill gives the attenuation due to viscosity, thermal conduction, and relaxation effects as

$$e^{-\delta\omega^2 z/c_o^3} \qquad (2)$$

$$\delta = \frac{4}{3}\frac{\mu}{\rho} + (\gamma - 1)\frac{k}{\rho C_p} + \frac{\mu'}{\rho}$$

and the bulk viscosity is approximately represented as

$$\mu' = 1.4 \times 10^{-3}\,\frac{\mu}{h^2}$$

where h is the ratio of the number of water-vapor molecules per unit volume to total number of molecules per unit volume of the atmosphere.

The temperature in the anechoic room was 105°F or greater for all heated jet tests, and the relative humidity was 30% or greater for all tests. Based on these limits of temperature and humidity, it was determined that, at 74 inches from the jet nozzle (the location of all the microphones), the attenuation was 2 dB at 64,000 Hz, and the dB level is reduced by a factor of 4 per octave. Therefore, it can be assumed that, if this representation for atmospheric attenuation is correct, no correction to the power level is required. It is interesting to note that, if temperature is reduced from 105°F to 70°F at 30% humidity, the correction is 12 dB at 64,000 Hz. This leaves unexplained the apparent low-power levels for the smallest nozzle; however, no other plausible explanation can be offered at present. Although the difference might be attributed to differences in initial turbulence level, there is no way to verify this.

Effect of temperature on total acoustic power.- As stated earlier, one of the objectives of this work was to find whether a reduction in radiated jet noise could be achieved at constant thrust and velocity by increasing temperature. If the sound power is written as

$$P = K\rho_j^n A V^8 \qquad (3)$$

where K contains effects of the ambient atmosphere and other factors,

and the thrust is taken as

$$\tau = \rho_j A V^2 \qquad (4)$$

then the power may be rewritten as,

$$P = K\rho_j^{n-1}\,\tau\, V^6 \qquad (5)$$

Now, if a normalized power is defined such that

$$P_N = \frac{P}{\tau V^6} = K\rho_j^{n-1} \qquad (6)$$

and the data for normalized power are plotted, the temperature (or density) law can be established. The data which were normalized in this manner are given in figure 7. Examination of these data shows quite a large amount of scatter. However, this is to be expected,

since the data were normalized to the 8th power velocity law, and minor variations from this law or minor measurement errors in velocity could easily cause the observed $\pm$ 3 dB variations in the normalized power level.

If a least-square curve is fitted to the data shown in figure 7, the slope is small, and for all practical purposes, the normalized power level can be said to be independent of temperature. Therefore, over the range of ambient to 1100°R, the sound power level of a jet exhaust is proportional to ρ_j (or inverse T_j).

This conclusion, then, would lead to the belief that there is nothing to be gained in noise reduction by heating the jet exhaust at constant velocity and thrust. That is, this conclusion can be drawn if it can be assumed that the temperature effect is linear to the highest practical operational temperature limits.

Since it was not possible to make tests at higher temperatures in the anechoic room because of valving and room cooling difficulties, the only practical way to determine the linearity of the temperature effect was to refer to previous tests. In reference 4 (as indicated in the Introduction), a series of tests was conducted at temperatures as high as 2800°R static temperature. Velocities ranged as high as 4000 fps and were as low as 880 fps. All the data are in terms of sound pressure level, and an empirical relationship is given for calculating SPL at any point in the near or far field. (There is an error in reference 4 which could lead to misuse of the data. On page 15, table I, the temperature given is total temperature and the speed of sound and velocity were mistakenly calculated based on total temperature instead of static temperature. It is also pointed out that the prediction formula for sound pressure requires total temperature instead of static temperature.)

It is possible to determine total sound power from the results of reference 4 if intensity ($I = \overline{P}^2/\rho c$ is assumed) is numerically integrated over a reference sphere. The formula for mean square pressure is

$$\overline{P}^2 = \frac{KT^s M^n (1 + \alpha^2 + M^2)^{5/2} (1 + \cos^4\theta) \left(\frac{C_1}{r^2} + \frac{C_2}{r^4} + \frac{C_3}{r^6}\right)}{\left[\left(1 - \frac{M\cos\theta}{1 + C_6 e^{-C_7 r}}\right)^2 + \alpha^2 M^2\right]^{5/2} \left(1 + \frac{C_4 e^{-C_5\theta}}{1 + C_6 e^{-C_7 r/4}}\right)} \tag{7}$$

For large values of r, the nondimensional (nondimensionalized to nozzle exit diameter) field distance (say $r > 20$), several terms may be discarded from this expression. On assuming large r, the equation becomes

$$\overline{p}^2 = \frac{C_1 KT^s M^n (1 + \alpha^2 M^2)^{5/2} (1 + \cos^4\theta)}{r^2\left[(1 - M\cos\theta)^2 + \alpha^2 M^2\right]^{5/2} (1 + C_4 e^{-C_5\theta})} \tag{8}$$

For calculating overall sound pressure, the parameters in the equation are

$$\left.\begin{aligned} C_1 &= M^{2.34} \\ KT^s M^n &= 4.63 \times 10^{-8}\, T^{1.54}\, M^4 \\ \alpha^2 &= .823 M^{-1.24} \left(\frac{T}{1000}\right)^{-2.3+1.47M} \\ C_4 &= 45.76 M^{2.11} \left(\frac{T}{1000}\right)^{3.37-2.39M} \\ C_5 &= 12.8 M^{-1.82} \left(\frac{T}{1000}\right)^{-1.79+1.16M} \end{aligned}\right\} \tag{9}$$

This expression was evaluated for power level, based on equation (1), in a small digital computer program. The correct units for ρc in equation (1) are lb-sec^2/in if used in conjunction with equations (8) and (9). The results of the power level calculations are shown in figure 8. The power level data are plotted against temperature for curves of constant velocity, which correspond to the velocity points for the tests discussed earlier in the report. It is quite evident that at temperatures up to 1200 or 1500°R, the assumption that power is inversely proportional to jet temperature is matched by the prediction method. However, at higher temperatures, the sound power falls off much more rapidly so that, at 3000°R, reductions are found that are 5 to 6 decibels more than would be achieved with an inverse temperature law.

From the standpoint of absolute magnitude, the agreement between total power levels calculated in this section and measured power levels from the tests described earlier is quite good, considering that the data were taken in two different environments. The tests reported here were anechoic, and the jet tests of reference 4 were free field with the jet directed upward. Figure 9 gives a comparison of the predicted total power and measured values for nozzle 3, which was 1.69 inches in diameter. To account for the increased nozzle size, 4.6 dB were added to the data from figure 7.

From the comparative standpoint, the prediction method has an overall V^7 law at low temperatures, as opposed to V^8 for the measured data presented in this report. However, from a comparison of absolute magnitudes, the prediction method seems to be accurate within 1 decibel. The data from the other three nozzles tested were similarly compared with the prediction method, and the comparison was found to be as good as that shown in figure 8, except for the smallest nozzle, which exhibited lower levels than predicted.

Since the prediction method, equation (8), was developed from a series of 21 different tests, with 70 measurement locations for each test, over a temperature range of 500°R to 2800°R, and since the prediction method is so accurate for low temperatures, the expected

reduction with high temperature is entirely believable. For all practical purposes, it has been demonstrated by the method from the study in reference 4.

Effect of temperature on directivity.- A directivity factor was developed for each test run to show the effect of temperature on directivity. However, for the temperature range studied in the experiments reported here (540°R - 1100°R), no correlated effect on directivity can be recognized in the data without prior knowledge of the expected trend.

Once again, resorting to the prediction technique developed in reference 4, the directivity factor is calculated for far-field radiation. The directivity factor, which is sound pressure level referenced to the calculated SPL at 90° to the jet axis, is shown in figure 10 for four different temperatures. The two curves at 540°R and 1100°R match the test data extremes. An average of the directivity factors, as determined by test, for all four nozzles for the two temperatures, is also shown in Figure 10. If the test data are examined alone, as stated above, no coherent effect can be attributed to temperature. However, an examination of the experimental data in conjunction with the predicted directivity curves shows that the agreement between experiment and prediction is quite remarkable. The experimental data do not vary more than 2 dB at any measurement point.

Examination of the predicted curves shows that, as temperature is increased, the peak in directivity factor shifts outward. Of course, this means somewhat decreased effectiveness in the overall power level reduction due to temperature increase, since the sound power will be directed more toward 90° as the temperature increases. This is not expected to affect the reduction by more than 1 dB, however.

Effects of temperature on frequency spectrum.- After examining a normalized octave spectrum of all the data, only minor changes in the spectrum shape can be attributed to temperature. In the two highest frequency bands, with center frequencies at 32 KHz and 64 KHz, the sound power level is observed to decrease by 1 to 3 dB as temperature is changed from 540°R to 1100°R at constant velocity. There is observed no shift in the spectrum peak and no change in the low-frequency bands.

Effects of Temperature on Simulated Fan Noise

It was speculated that the addition of heat to the bypass air of a fan engine exhaust would not only change the character of the jet noise but would also significantly affect the propagation of fan tones through the heated region. The only sure way to determine the effects would involve testing of a full-scale or model fan engine, but precluding this because of expense, it was possible to get a qualitative evaluation of the effect in the laboratory.

Schematically, the proposed modification to an engine would be as shown in figure 11a. A diffuser would be added to the fan duct to slow the fan air, and then fuel would be injected and burning would occur. An acoustic schematic of the engine (figure 11b) shows that fan noise is generated in medium 1, which then must refract through the burning boundary into medium 2, and then later through the jet mixing boundary and into medium 3.

A simple experiment was designed to obtain order of magnitude effects of the high-temperature region on pure tone propagation. In this experiment, a co-annular jet was constructed in an anechoic room. The room dimensions from wedge tip to wedge tip were

approximately 12 x 12 x 19 feet, and the jet exhausted 8 feet from the ceiling exhaust muffler which ejected air into the double-walled cavity surrounding the anechoic room. The temperature of both the primary and secondary air jets could be individually controlled from ambient to approximately 800°F. The secondary jet was constructed, as shown in figures 12 and 13, so that four acoustic driver units were used to introduce pure tones into the secondary flow upstream of the nozzle exit plane. The tubes connecting the driver units and the secondary jet were wrapped with a water jacket to keep the tube walls cool. When hot air was supplying the secondary jet, a very small amount of cooling air was introduced into the driver unit tubes to prevent the hot air from flowing from the boundary layer into the driver unit tube. This cooling feature in the driver tubes permitted a relatively steep gradient in the temperature between the ambient air in the driver tube and the high-temperature air in the secondary flow. Although this is not the exact acoustic analogy of figure 11b, it does provide a sound wave which refracts through two temperature gradients, as would happen in the actual engine design. Further, if the speakers are operated in all possible phase combinations, two angular (or tangential) acoustic modes can be simulated, and when all drivers are in phase, the plane-wave mode is approximated.

A series of tests was run wherein the secondary air temperature was varied, while flow Mach number was held constant. Another series of tests was run and secondary temperature was varied for constant velocity. The constant Mach number runs were made since Mach number is the parameter in duct-mode propagation theories. With constant Mach number, all duct effects should be eliminated except for those attributed to temperature. The results of these tests are described below.

Effect of secondary flow temperature on pure tone propagation-data analysis.- For each flow and temperature condition listed in the Table II test summary, radiated sound pressure level was recorded in the far field at six angular positions beginning at 15° and continuing every 15° through 90°. The SPL was recorded first with the drivers off and then for each of the three driver phase combinations simulating the (0, 0) mode, the (1, 0) mode, and the (2, 0) mode. Sound pressure level was simultaneously recorded in three of the four driver-unit tubes.

When a pure tone was introduced into the nozzle during the tests, the control and data acquisition system was as shown in figure 14. During a given test run, the drivers were set in the desired phase combination, and a frequency sweep was made from 400 Hz to 8000 Hz with constant electrical input to the acoustic drivers. All data, including the oscillator signal, were recorded on magnetic tape. After the test, the data were analyzed as illustrated by the block diagram in figure 15. In the analysis, a narrow-band analyzer was used to improve the pure tone signal-to-noise ratio, and the frequency response of the annular-duct radiation field was displayed on an X-Y plotter.

It was expected that three individual effects could be evaluated, at least qualitatively, as a result of the pure tone tests described. It was anticipated that (1) higher-order duct-mode cuton frequencies would be increased as duct temperature increases, (2) directivity of the pure tone radiation would change with flow temperature, and (3) the level of the pure tone wave propagating through the high temperature medium would change with temperature. Each of these three effects are discussed below.

Effect of temperature on higher acoustic duct mode cuton frequency.- In the absence of a sheared flow and viscous losses, the wave equation for propagation through an annular

duct is (see, for instance, ref. 6) the Bessel's equation of order m

$$\frac{d^2P}{dt^2} + \frac{1}{r}\frac{dp}{dr} + \left\{k^2\left[(1 - MK)^2 - K^2\right]\frac{-m^2}{r^2}\right\}P = 0 \tag{10}$$

where $K = \frac{\gamma}{j\omega/c} = \frac{\gamma}{jk}$

r is the propagation vector
M is the flow Mach number
m is an angular wave vector which must be an intega because of periodicity.

The solution to this equation, including the angular modal distribution, is

$$P = \left[A\, J_m(k_r r) + BN_m(k_r r)\right] \cos m\,\theta \tag{11}$$

and the eigenvalues,

$$k^2_{r_{mn}} = k^2\left[(1 - MK)^2\right] - K^2 \tag{12}$$

are determined from the impedance relationship at the boundaries. For rigid walls, $Vr = 0$ and the roots of the relationship

$$J'_m(k_r t)N'_m(kr) - J'_m(kr)N'_m(k_r t) = 0 \tag{13}$$

establish the eigenvalues $k_{r_{mn}}$. It is observed that

$$\omega_{mn}/\text{cuton} = k_{r_{mn}}\, c \tag{14}$$

and it is seen that the cut-on frequency, ω_{mnc}, of a particular mode, mn, is directly proportional to the speed of sound of the medium within the duct. Since the speed of sound is proportional to $\sqrt{T}$, the cut-on frequency of a particular duct mode should increase in direct proportion to the square root of duct temperature.

The main point of this discussion is that the cut-on frequency of any duct mode, other than the plane mode, is increased as the square root of temperature. This fact could be particularly useful if the fan happened to be generating a pressure distribution which was predominately propagating in a mode at or just above its cut-on frequency. If the cut-on frequency of this mode were raised by duct heating to a frequency greater than the frequency of the fan pressure distribution, then it was speculated that a significant attenuation would be evidenced in the radiated noise.

This behavior was verified to some extent in one phase of the testing. For instance, when

alternate driver units were out-of-phase, a (2, 0) mode pressure distribution was simulated. For this pressure pattern, as frequency is increased, the point at which significant pure tone radiation begins is the cut-on frequency of the (2, 0) mode. First, it is interesting to show the radiation characteristics of the duct/nozzle combination in the (2, 0) mode with no flow and at ambient temperature. Figure 16 shows the "normalized" radiation response of the test duct when excited by a simulated (2, 0) mode pressure distribution. To normalize the radiated SPL, the SPL measured in one of the acoustic driver-unit tubes was subtracted from the radiated SPL. This gives the radiated SPL for a constant-amplitude sound pressure at the source. Of course, it makes no assumption about interaction of the thermal barrier and the source output. It is highly probable that the sound pressure at the microphone in the driver tube contains a significant component of reflected wave and that the reflected wave contribution will change as the temperature of the secondary air changes. Realistically, therefore, the radiated SPL should be normalized to the source SPL instead of source SPL plus reflected wave; however, unless the reflected component is estimated analytically, this is not possible. Since it was not practical to eliminate the reflected component in the normalization process, *the possibility of reflected waves biasing the results must be kept in mind throughout the* remainder of this discussion.

Referring again to figure 16, it is observed that significant radiation at a point 15° from the jet axis begins at approximately 1550 Hz for no-flow and ambient temperature in the duct. The calculated cut-on frequency (using the tables in reference 7) for an infinite length annular duct with a .5 hub/tip ratio, in the (2, 0) mode is 1360 Hz. This is approximately 200 Hz lower than the measured value, but the test duct was fitted with a conical nozzle which reduced the 8-inch duct diameter to 3.5 inches. The addition of the smaller-diameter conical nozzle would certainly tend to increase duct cut-on frequencies. The shape of the normalized radiated SPL is similar at all six angular positions but varies somewhat in amplitude.

Next, to show the effect of flow and temperature on the (2, 0) mode cut-on frequency, the normalized radiated SPL is shown in figure 17 at the same field position as in figure 16. Here, the radiated pure tone level became lost in the jet noise at about 1550 Hz for the 530°R case and at 2000 Hz for the 1260°R case. Therefore, the shape of the cutoff curve was superimposed from the no-flow condition. Examining the response of the duct at constant Mach number, it is evident that increasing temperature increases cut-on frequency. From the theory, with an increase in temperature from 530 to 1260°R (at the indicated velocities, a static temperature ratio of 1213/510), the frequency should increase by the square root for the temperature ratio, 1.54. The actual increase of the (2, 0) mode cut-on frequency is approximately 1.3.

Effect of heating on radiated pure tone SPL. - To show the effect of heating on radiated SPL, the difference between normalized radiated SPL for the ambient and 800°F cases is determined. Representative plots are shown in figures 18, 19, and 20 at three angular positions 25 diameters from the exit plane. The difference plot is shown from a frequency beginning at the (2, 0) mode cut-on frequency for the high-temperature case. Below this frequency, the difference can only be estimated but is of the order of 20 decibels, down to the cut-on frequency of the (2, 0) mode at ambient temperature. Below this frequency, the difference curve would be meaningless. The difference curves show that, over the greater part of the frequency range, SPL is reduced (of course, remembering that these data are referenced to a constant source level - if the increase in temperature changes the source output noise level, these trends are also subject to change). If a frequency is carefully chosen, large

reductions in pure tone level can be achieved, but obviously for other frequencies, an increase would be observed in radiated SPL. Only at a point 90° to the jet axis does the increase in temperature show an attenuation across the complete frequency spectrum. Therefore, based on these data, it is difficult to draw firm conclusions concerning the effect of temperature on the attenuation (or gain) in level of a pure tone refracting through a moving, high-temperature layer of air.

Effect of temperature on pure tone directivity.- The general effect of jet heating on jet noise directivity is to increase the angle, referenced to the jet thrust axis, of maximum sound pressure radiation, and it was expected that the effect on pure tone radiation through the heated jet would follow the same trend. Unfortunately, the data taken do not seem to show any particular trend. Figures 21, 22, and 23 are typical of the directivity data. These data are taken from the normalized radiated SPL when the driver units were phased to simulate the (2, 0) mode. Assuming that the directivity trends for a circular duct are representative of those for an annular duct, at frequencies sufficiently high enough above the cut-on frequency for a mode, the radiation patterns will be multi-lobed. Therefore, any straight line or faired curve which connects the data taken at 15° intervals is highly questionable. Due to the lack of calculations showing the radiation trend to be expected from a cold annular jet with flow, it is difficult to compare the radiation patterns for a hot jet and a cold jet and to comment on the trends. The data in figures 21, 22, and 23 seem to be highly uncorrelated, and general conclusions are meaningless without a thorough experimental program where data are measured every 5 degrees, or a theoretical analysis to calculate radiation patterns.

If a model fan engine with an afterburner is built, it will be possible to evaluate the effect of heating on directivity for the particular frequencies generated by the fan if enough data are taken in the far field. However, use of the model data to predict full-size effects should be supported by a theoretical analysis and computer parameter study.

POSSIBLE APPLICATION OF JET HEATING

The tests described in the previous section, have shown that heating is a potential way to reduce both jet noise and fan-generated noise propagating through a high-temperature region in the fan duct. In present bypass fan engines, where the secondary air flow is at nearly ambient temperature, it would be possible to achieve a jet noise reduction on the order of 6 decibels by heating the air to 3000°R.

Obviously, a 6 db reduction in jet noise would not mean much if the fan noise were as loud as that generated by present-day power plants, but once current-technology fan noise reduction techniques are applied, the jet noise will again be audible, at a perceived noise level far louder than the 80 EPNdB noise floor set as a goal by the FAA (ref. 8, part 36.201-a-1). Since even the "quiet" engines presently in the design stage (Kramer - ref. 9) will have a jet-noise floor about 93 PNdB on takeoff, a potential 6 dB jet noise reduction would appear to be highly attractive. On more conventional engines, such as that used on the DC-8 jet, noise reduction techniques are certainly required. A press release discussing recent DC-8 flight tests of the nacelles designed under NASA contract (ref. 10) reports "preliminary results indicate the new nacelles were an outstanding success; on the landing approach the first noise heard from the aircraft is the jet exhaust noise; fan noise has for all practical purpose been eliminated." These impressions highlight the fact that jet noise must not be forgotten.

In addition to the jet noise reduction available from heating, there also appears to be a potential for reduction of fan noise. As shown in figures 18, 19, and 20, reductions of as much as 10 db in radiated pure tones were measured at some frequencies. While further research is required in this area, it is certainly a promising avenue of approach.

Based on these results, it was determined that the most promising demonstration of jet heating would lie in the modification of an existing fan-jet engine, with test-stand operation to determine acoustic characteristics before and after modification. The specifications of a number of existing and proposed fan-jet engines were reviewed as candidates for application of duct heating. The CF 700 was chosen for a design study to determine the problems involved in installing a duct burning cycle which meets all the acoustical requirements. This engine was not chosen because of any superior performance or noise characteristics but simply because it was (1) a production fan jet engine and would be readily available to conduct a test-stand demonstration, and (2) it has a relatively low thrust which makes operation more economical and the test stand and test site less expensive.

Because of the rather indefinite conclusions which can be drawn concerning the magnitude of fan noise reduction (or possibly increase) to be expected, it is felt that a further test with a model fan engine and simplified burner or perhaps even a resistance heating stage would be more profitable and less expensive. However, to investigate some of the anticipated non-acoustical problems of modifying a jet engine to demonstrate noise reduction through heating, design studies were performed for full-scale testing. Through this approach, the design of a modified engine would be well underway should it be decided to test a full-size engine, or if the less sophisticated model were chosen for testing, the analysis developed could readily be applied to its design.

It was desirable that the analysis be done for a test rig that would model realistic hardware using existing technology. An estimate of the difficulty of incorporating various aspects of realistic hardware in the design could be ascertained from such a study. Furthermore, this was considered the best way to estimate the effect on the acoustic phenomena being tested which might result from simplifications made to ease the difficulty of testing.

Figure 24 is an artist's conception of a fan-jet engine modified for duct heating. The modification would essentially consist of an extension of the primary flow nozzle, a wide-angle diffuser for slowing the fan-stage air (screens or other devices are required to enhance the wide-angle diffusion characteristics but are not shown in this illustration), a burner stage, and a variable-geometry exhaust nozzle (not depicted) to permit operation with or without burning.

Requirements For Application

As a result of the possible application to existing turbofan engines, it became apparent that several areas of engine design required intensive study. Also, some problems which may normally occur (e.g., combustion instability) require different handling because of possible effects on engine noise characteristics.

High-frequency combustion instability was studied in some detail, since this can be a serious problem in a test rig or an actual engine. Although a common approach taken to eliminate high-frequency combustion instability is to use acoustic liners, this technique will not be available in the testing discussed. These tests will be conducted primarily to observe and measure an acoustic phenomena, and acoustic liners would affect the results. Further-

more, the effect of the liner on the acoustic phenomena would not be easy to isolate, since the liner would behave differently during burning and nonburning. It would not be practical, for instance, to run cold and ascertain the effect of the liner and then to subtract this effect from the results obtained while burning.

The results of the analytical design studies are presented in Appendix A, and the combustion instability analysis is contained in Appendix B. Although some of the material may be considered routine by engine designers, quite a bit of research was devoted to many topics. Appendix B is an original treatment of combustion instability of annular chambers.

CONCLUSIONS AND RECOMMENDATIONS

It is predicted that significant jet noise reduction can be achieved if the bypass fan air is heated from near ambient to the region of 2500-3500°R. This assumes that, for the engine being discussed, the noise generated by the fan jet exceeds the noise generated by the primary jet (as is usually the case). The predicted jet noise reduction is based on results from a semi-empirical jet noise prediction method with proved accuracy in the 500-1100°R temperature range.

It was shown that fan-generated tones might be reduced significantly by the application of fan-duct burning. However, the fan noise could not be realistically simulated using acoustic driver units. It was also not possible to create a satisfactory interface between the hot and cold regions in the same manner as would occur in fan duct burning. Consequently, further experimental and analytical work is necessary to validate and evaluate the reduction.

It is recommended that a model consisting of a fan and burner system be tested. The model should be instrumented so that thrust may be measured directly as well as calculated from pressure and temperature measurements to eliminate any possibility of error in determining thrust and average exhaust velocity.

TABLE I. PARAMETERS FOR HEATED JET TESTS

Controlling Parameters						*Nozzle Size and Number			
T_T °R	P_T psig	V_E fps	T_E °R	V_E	T_E	0.93" D (1)	1.20" D (2)	1.69" D (3)	2.00" D (4)
569	17.14	600	540	597	539	1	1	1	1
730	16.54	600	700	607	700	1	4	2	1
929	15.96	600	900	610	899	1	1	2	2
1128	15.61	600	1100	604	1099	0	1	1	1
592	19.77	800	540	801	539	2	4	1	1
753	18.51	800	700	808	700	2	1	1	1
952	17.46	800	900	815	899	1	1	1	1
1151	16.86	800	1100	812	1099	0	1	1	1
622	23.61	1000	540	1007	538	1	1	1	1
783	21.30	1000	700	1015	699	1	4	2	1
981	19.52	1000	900	1013	899	1	1	1	2
1179	18.51	1000	1100	1018	1098	0	0	1	1
819	25.06	1200	700	1220	698	2	1	1	1
1017	22.28	1200	900	1219	898	1	1	1	2
1214	20.62	1200	1100	1219	1098	0	0	1	1
1059	25.81	1400	900	1421	898	2	0	2	1
1255	23.34	1400	1100	1421	1097	0	0	1	1

*Numbers in column under nozzle size indicate number of runs at that particular test condition.

TABLE II. TEST CONDITIONS FOR DEMONSTRATING EFFECT OF SECONDARY FLOW TEMPERATURE ON RADIATED PURE TONES

Primary Flow				Secondary Flow			
Total Pressure psi	Total Temp. °R	Velocity fps	Mach No.	Total Pressure psi	Total Temp °R	Velocity fps	Mach No.
*0	530	0	0	0	530	0	0
**0	530	0	0	0	530	0	0
5	660	840	.70	2	530	487	.44
↓	↓	↓	↓	↓	660	544	↓
↓	↓	↓	↓	↓	860	620	↓
↓	↓	↓	↓	↓	1060	688	↓
↓	↓	↓	↓	↓	1260	751	↓
5	860	960	.70	2	530	487	.44
↓	↓	↓	↓	↓	660	544	↓
↓	↓	↓	↓	↓	860	620	↓
↓	↓	↓	↓	↓	1060	688	↓
↓	↓	↓	↓	↓	1260	751	↓
5	860	960	.70	5.5	530	751	.70
↓	↓	↓	↓	4.2	660	↓	.62
↓	↓	↓	↓	3.1	860	↓	.54
↓	↓	↓	↓	2.45	1060	↓	.48
↓	↓	↓	↓	2.0	1260	↓	.44
5	1060	1066	.70	2	530	487	.44
↓	↓	↓	↓	↓	660	544	↓
↓	↓	↓	↓	↓	860	620	↓
↓	↓	↓	↓	↓	1060	688	↓
↓	↓	↓	↓	↓	1260	751	↓

* For this test the nozzle was completely blocked so that secondary sound radiation from the driver units and piping could be determined.

** This test was used to determine the no-flow acoustic radiation characteristics of the annular duct when excited by the plane mode, the (1.0) mode and the (2.0) mode.

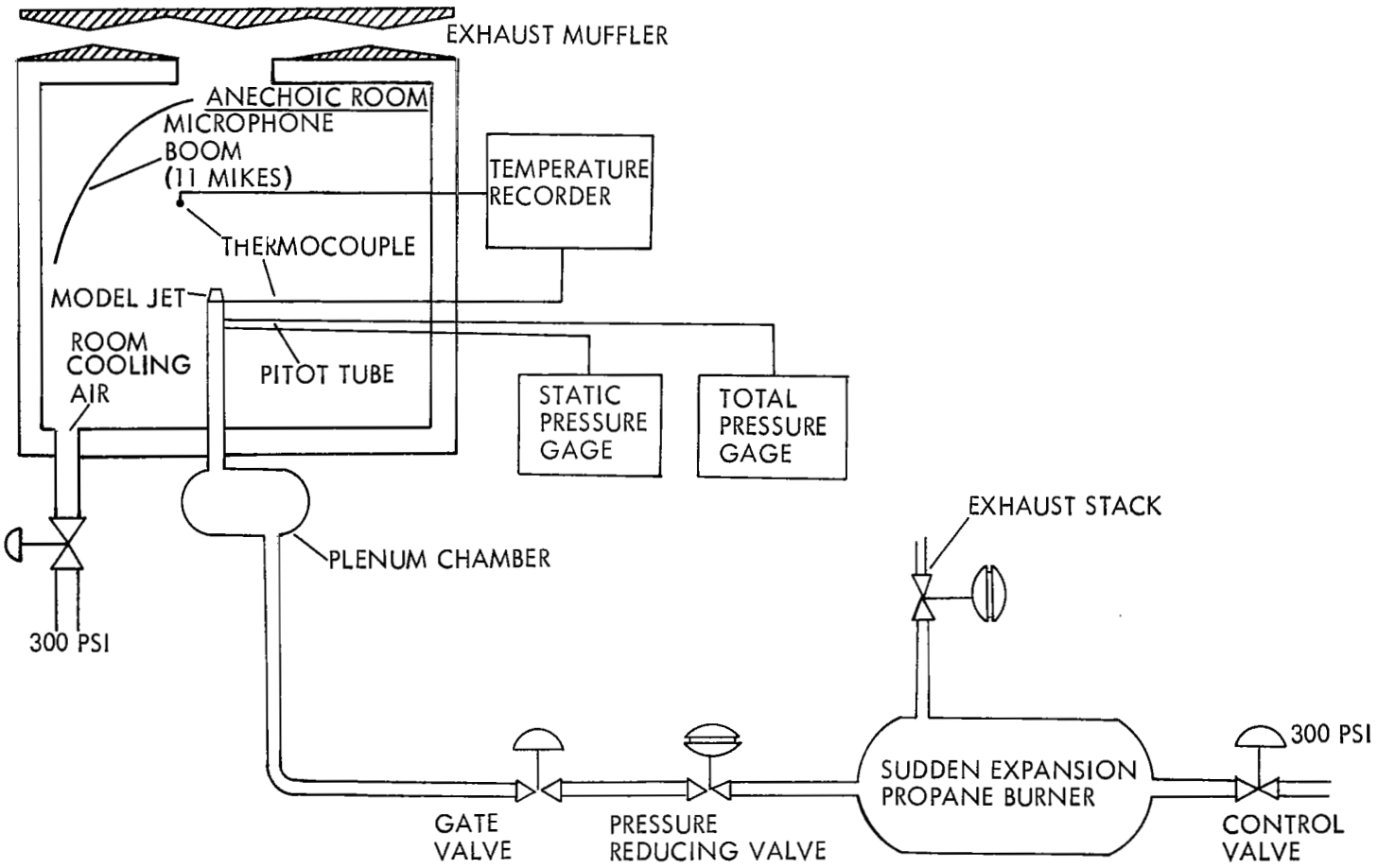

FIGURE 1 SCHEMATIC OF TEST SET UP

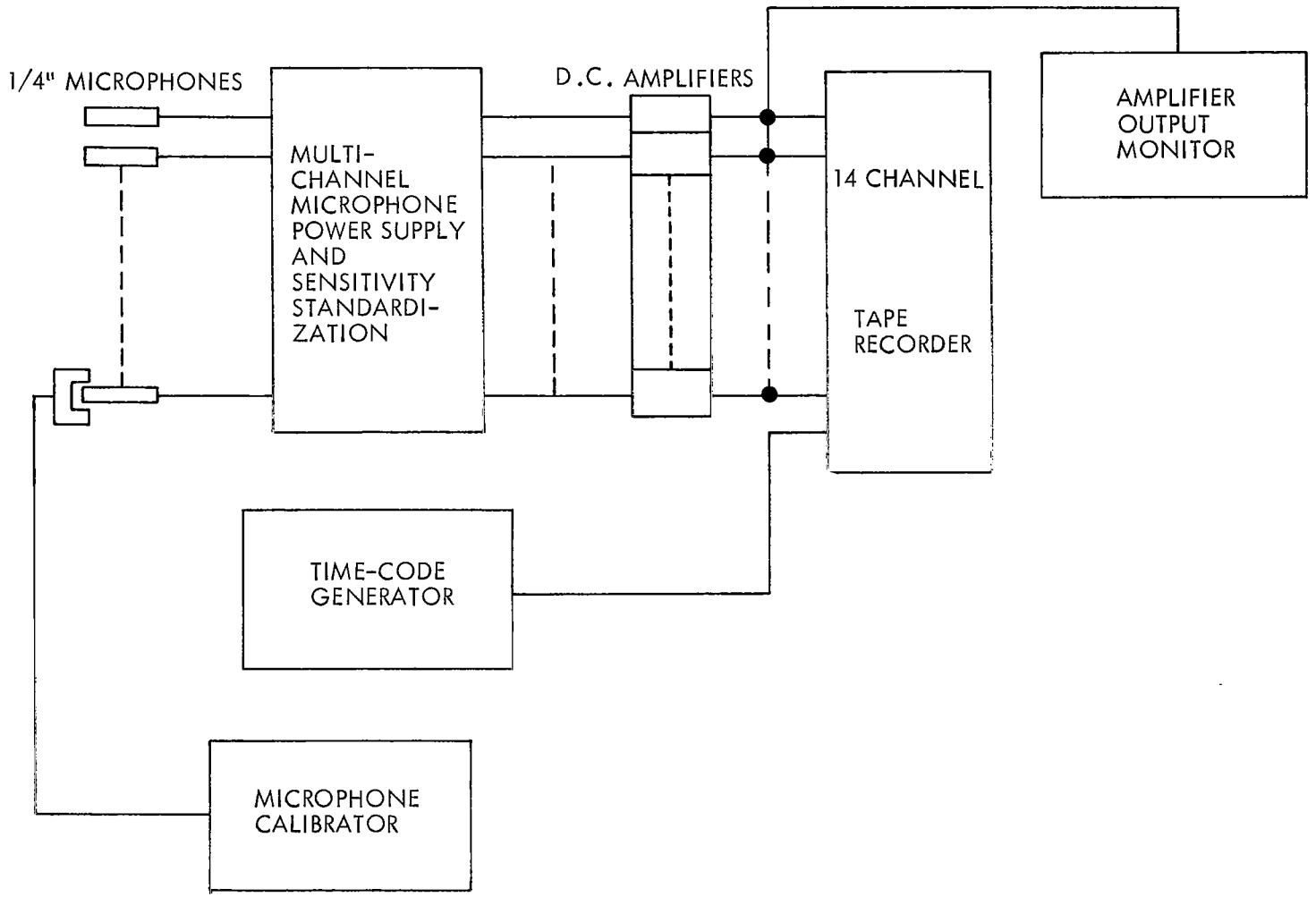

FIGURE 2 SOUND PRESSURE LEVEL DATA RECORDING AND CALIBRATION SYSTEM

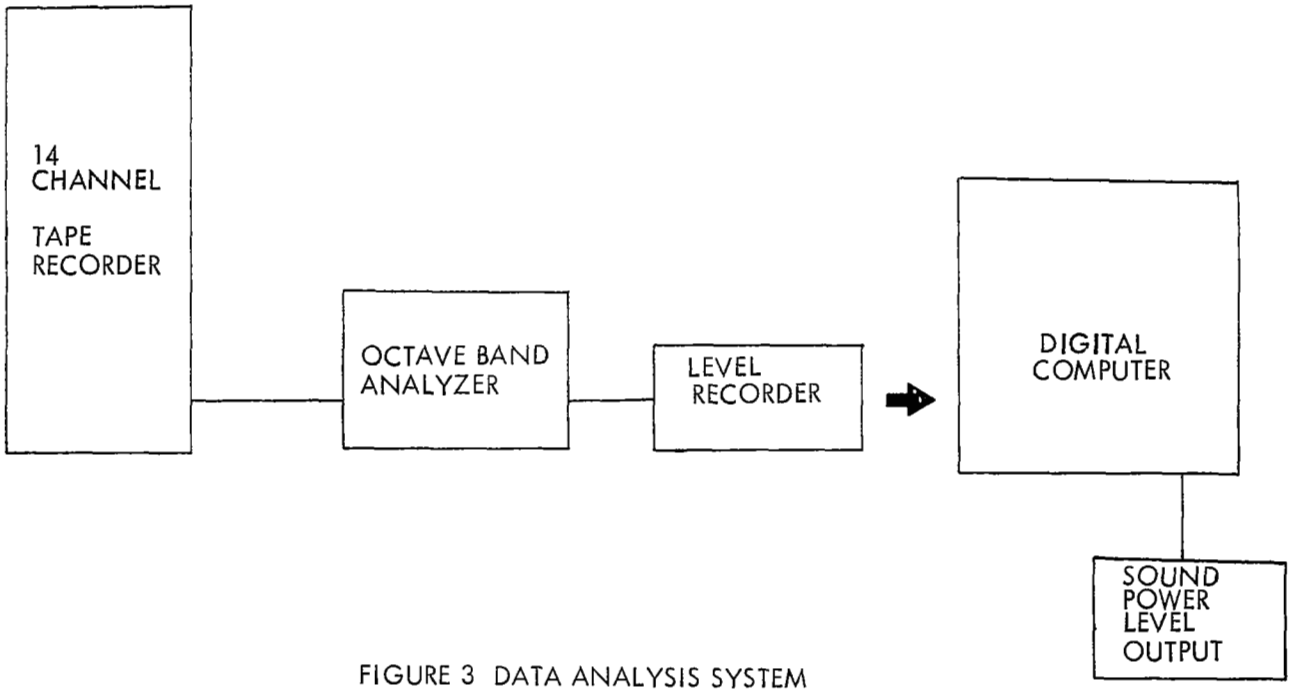

FIGURE 3 DATA ANALYSIS SYSTEM

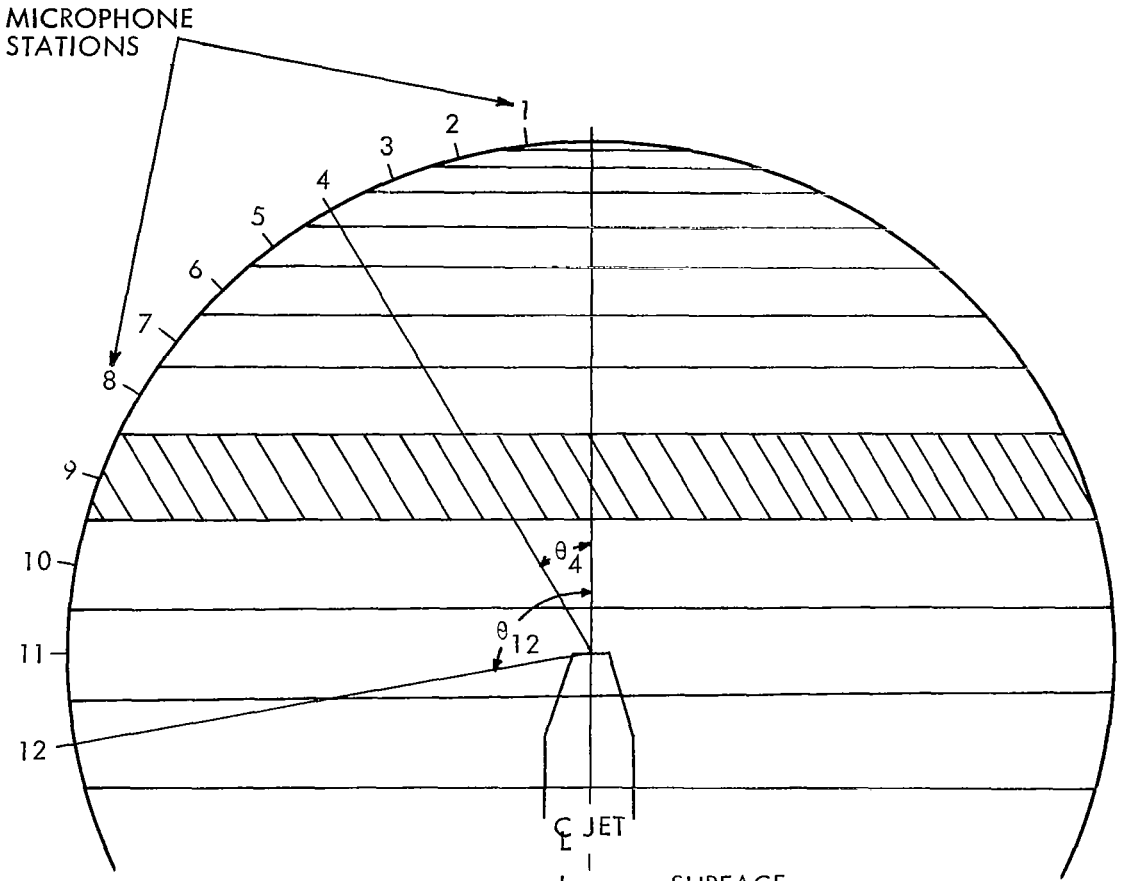

STATION NO., n	ANGLE, θ_n	SURFACE AREA OF SPHERICAL SEGMENT, SQ. FT.
1	7.5	3.96
2	15.0	7.90
3	22.5	11.68
4	30.0	15.25
5	37.5	18.56
6	45.0	21.56
7	52.5	24.19
8	60.0	30.95
9	70.0	38.97
10	80.0	40.84
11	90.0	41.46
12	100.0	40.84

FIGURE 4 MICROPHONE STATIONS AND AREAS USED FOR CALCULATING POWER

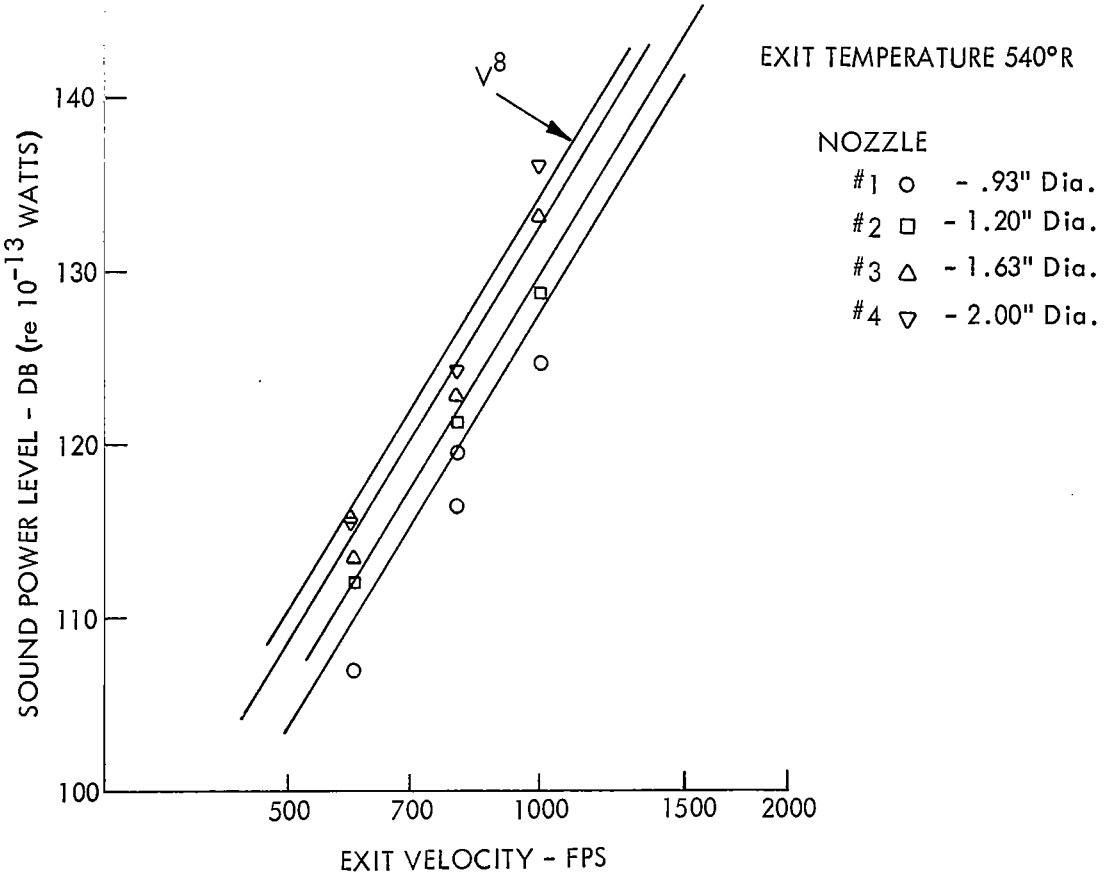

FIGURE 5 EFFECT OF VELOCITY ON SOUND POWER LEVEL - EXIT TEMPERATURE 540°R

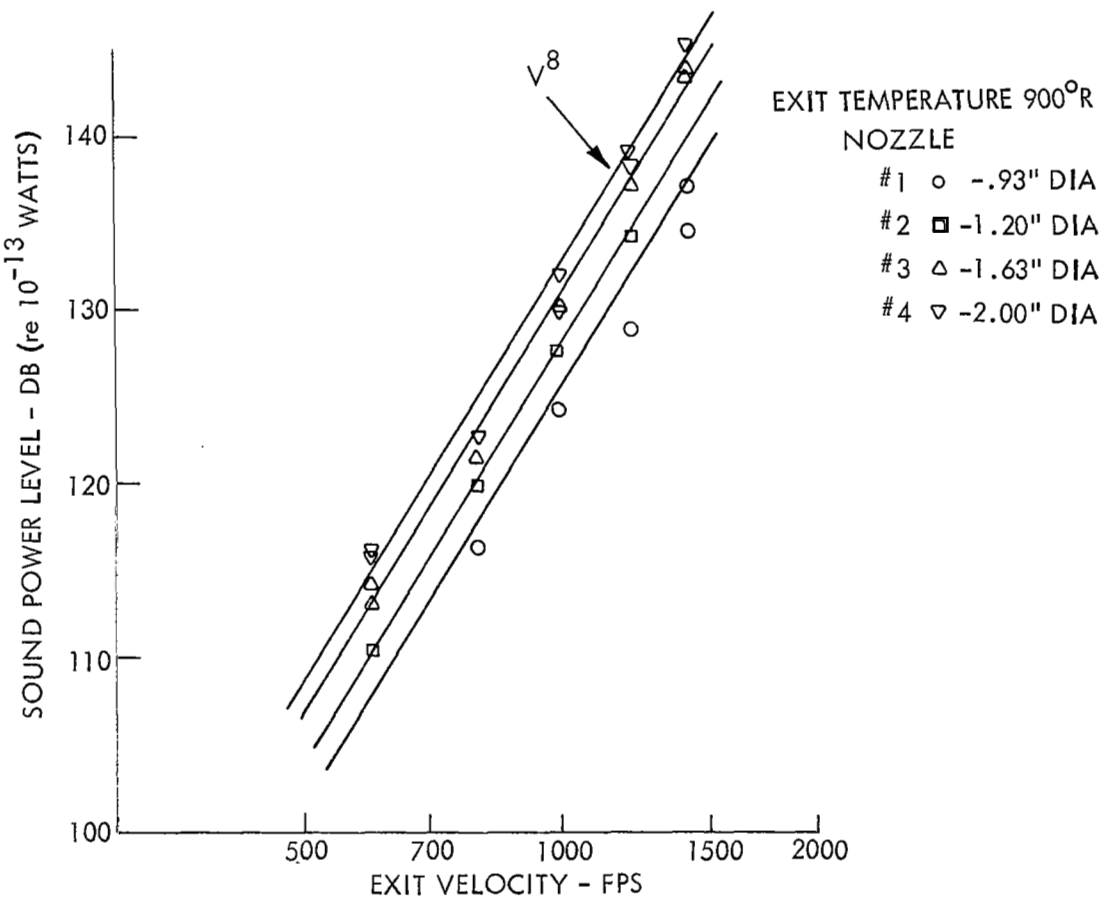

FIGURE 6 EFFECT OF VELOCITY ON SOUND POWER LEVEL - EXIT TEMPERATURE 900°R

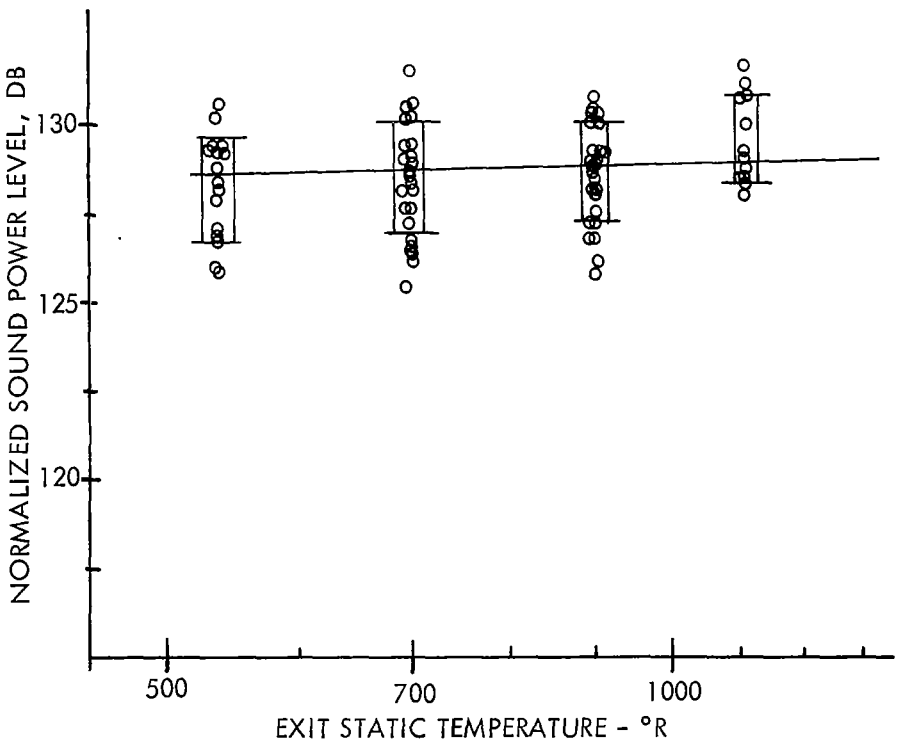

FIGURE 7 SOUND POWER LEVEL NORMALIZED TO $\rho_i AV^8 = \tau V^6$

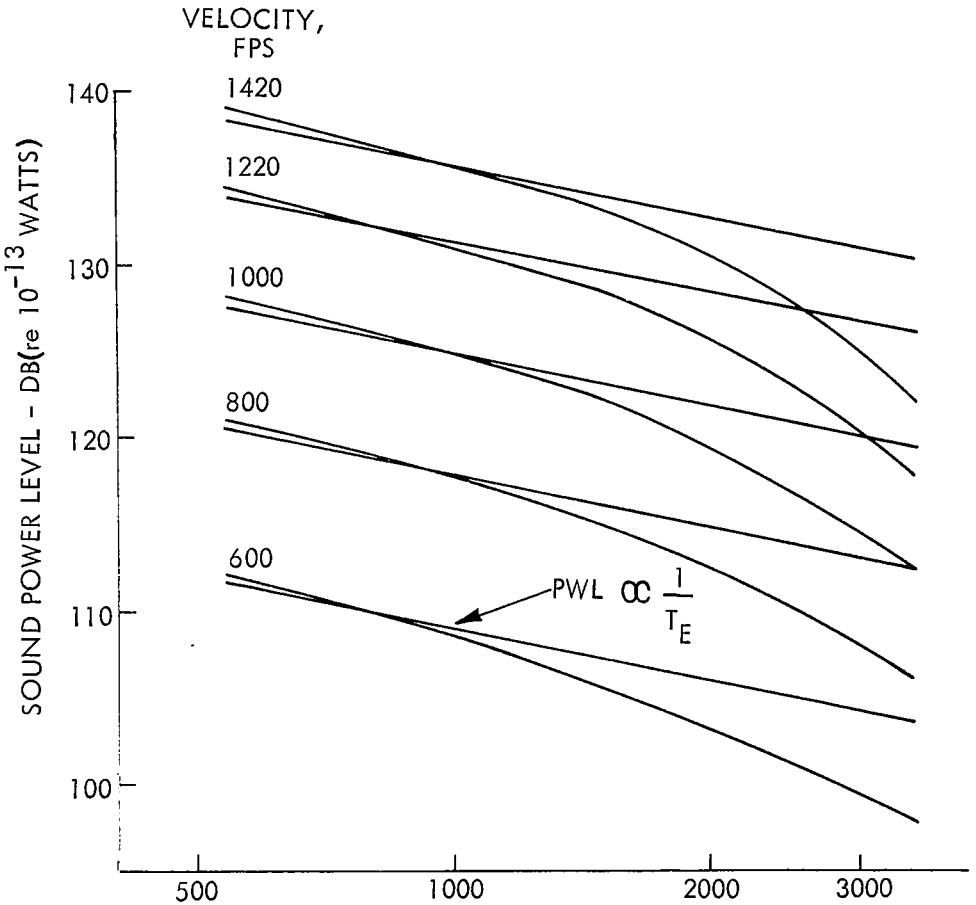

FIGURE 8 EFFECT OF JET TEMPERATURE ON TOTAL SOUND POWER FOR 1" NOZZLE (FROM REFERENCE 1)

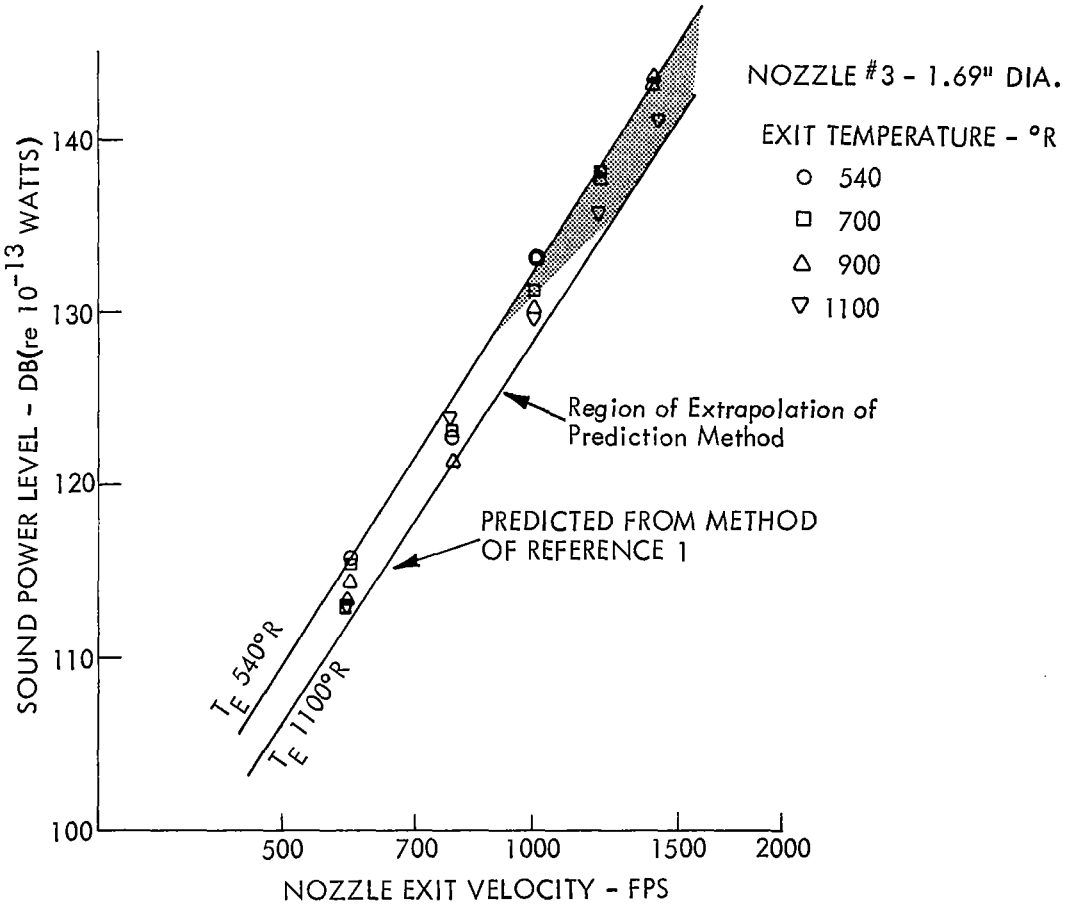

FIGURE 9 COMPARISON OF MEASURED SOUND POWER LEVEL AND PREDICTION METHOD

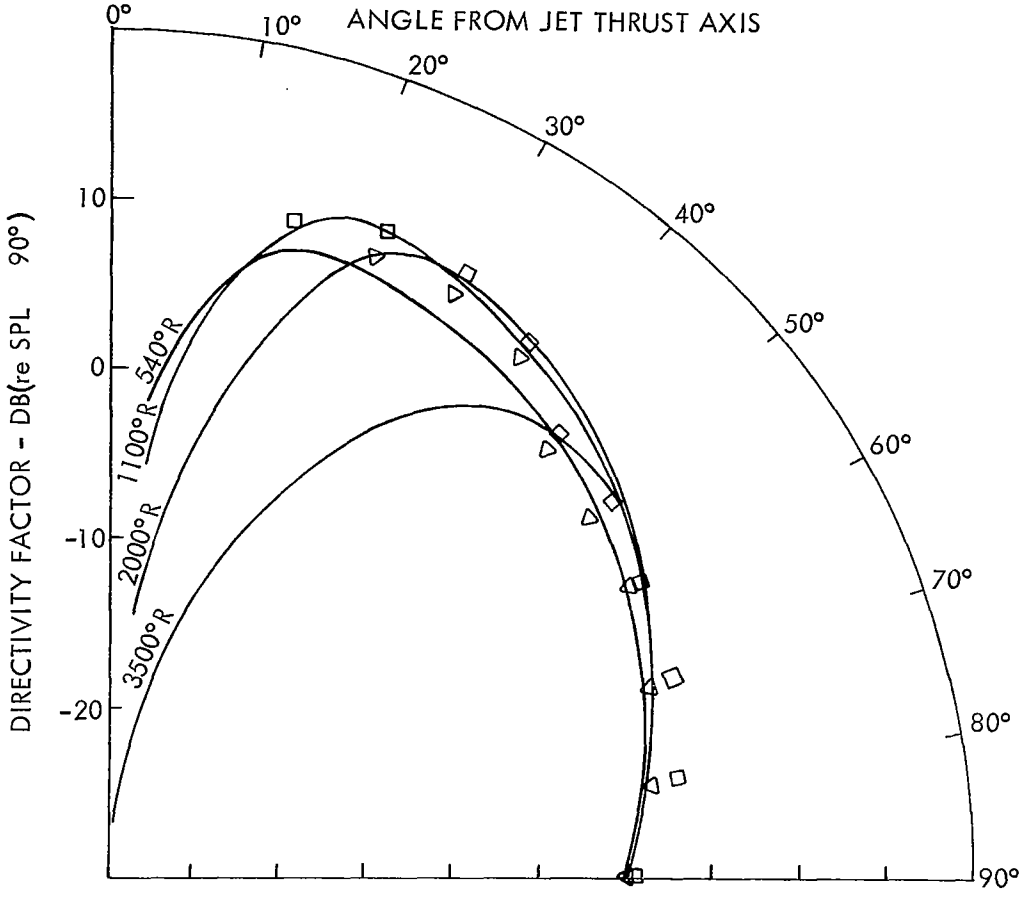

FIGURE 10 EFFECT OF TEMPERATURE ON DIRECTIVITY FACTOR - COMPARISON OF PREDICTION METHOD WITH MEASURED DATA

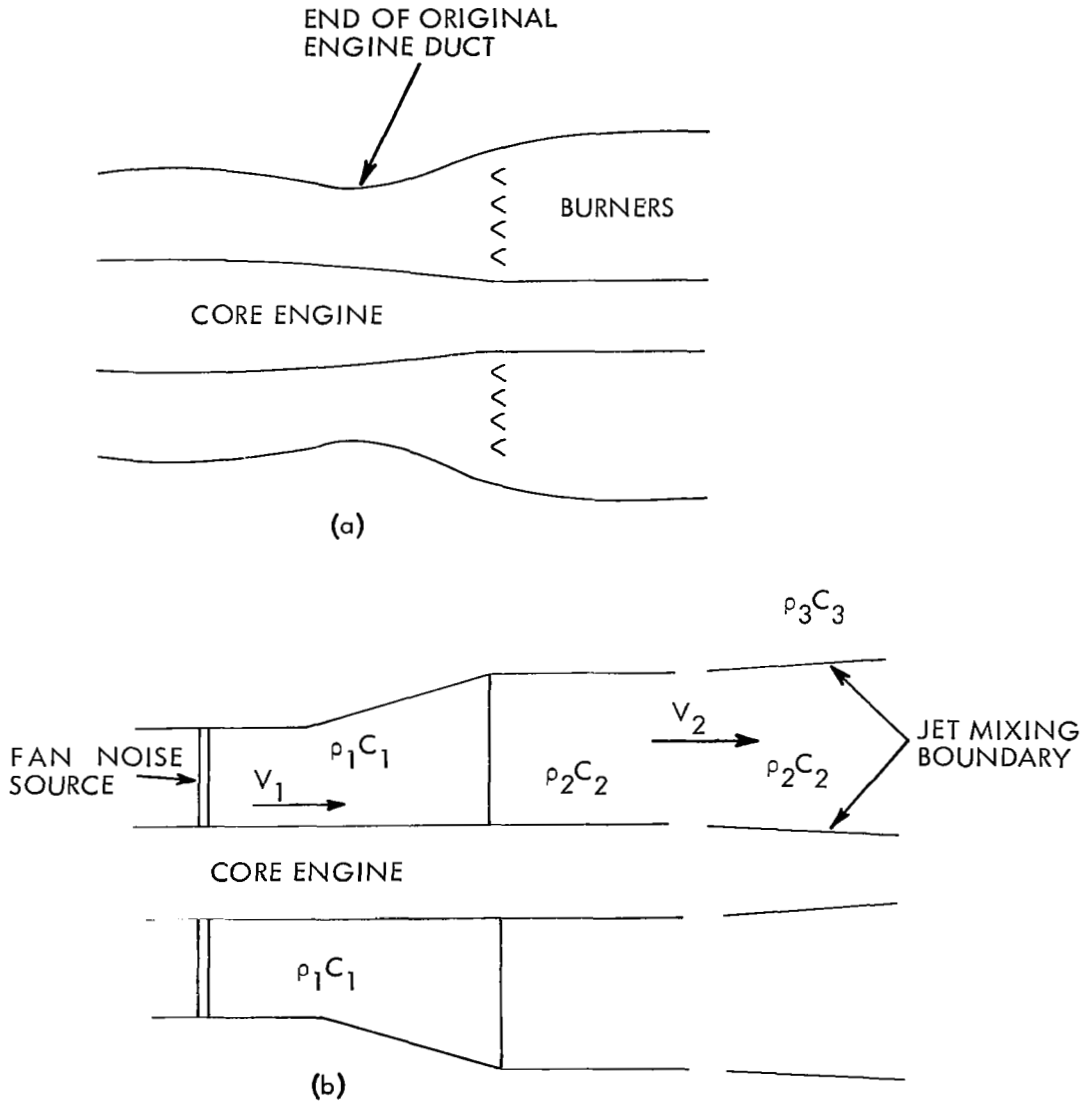

FIGURE 11 SCHEMATIC OF FAN ENGINE WITH DUCT BURNING

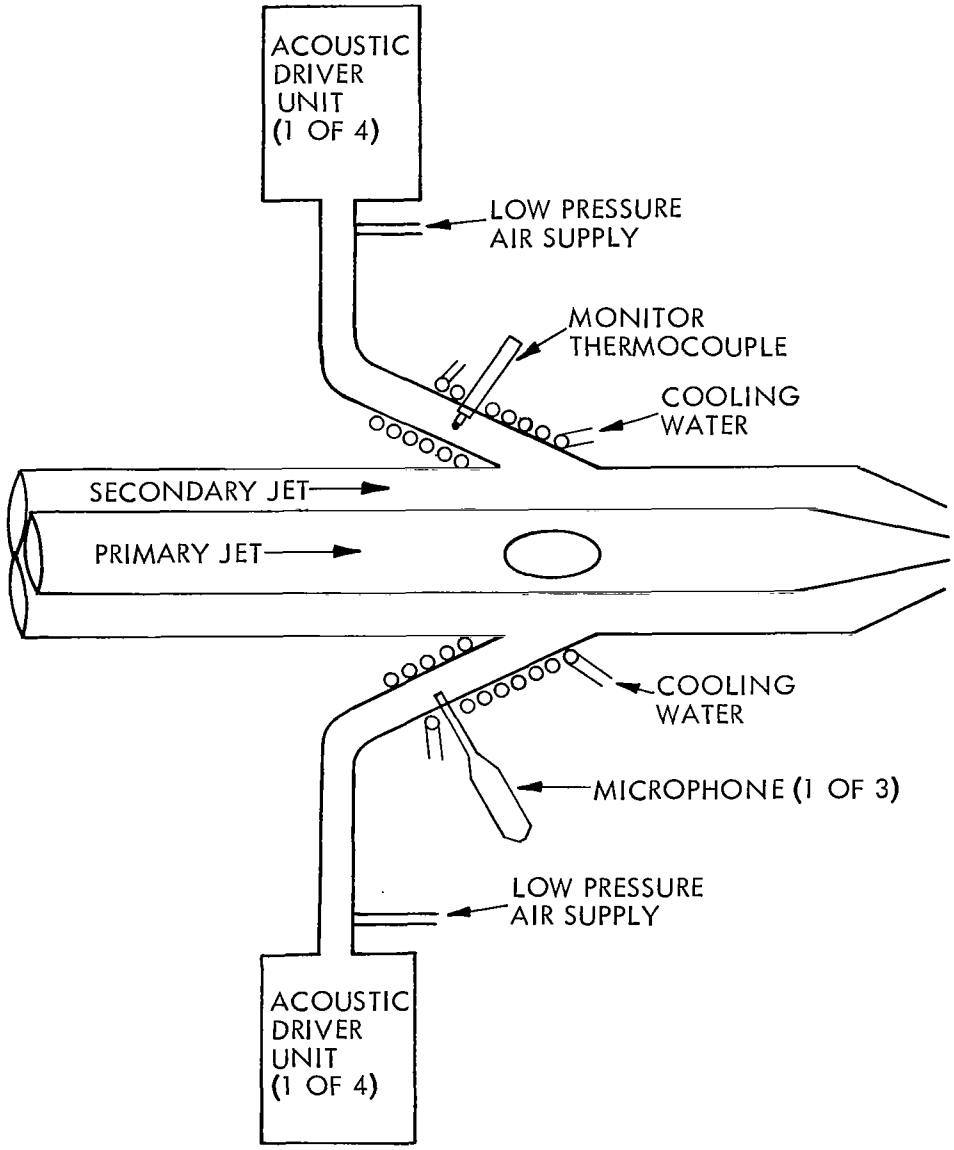

FIGURE 12 SCHEMATIC OF TEST SET UP TO EVALUATE EFFECT OF BYPASS AIR HEATING ON PURE TONE SOUND RADIATION

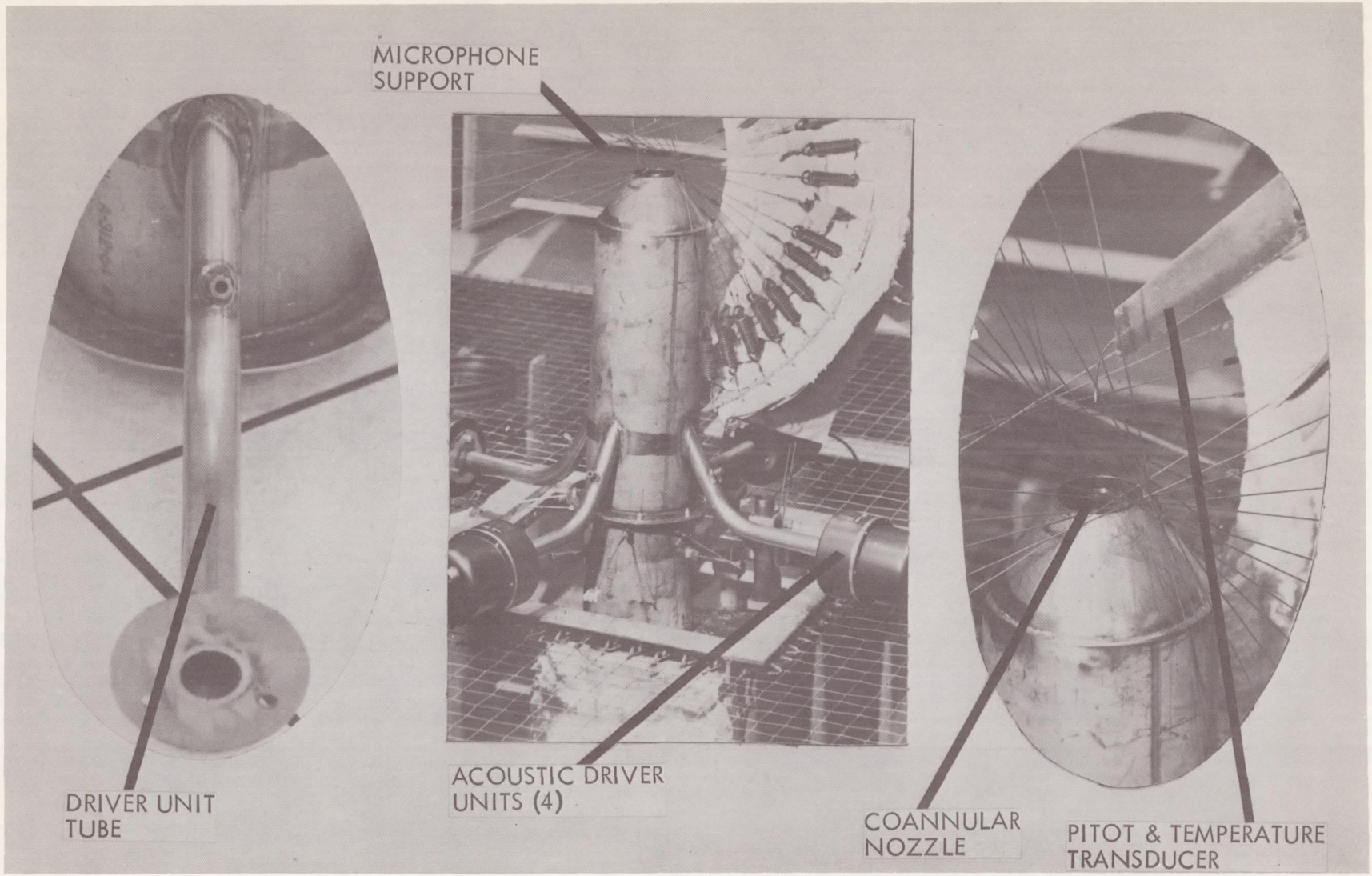

FIGURE 13 MODEL JET NOZZLE SET UP FOR DETERMINING TEMPERATURE EFFECTS ON RADIATED PURE TONE NOISE

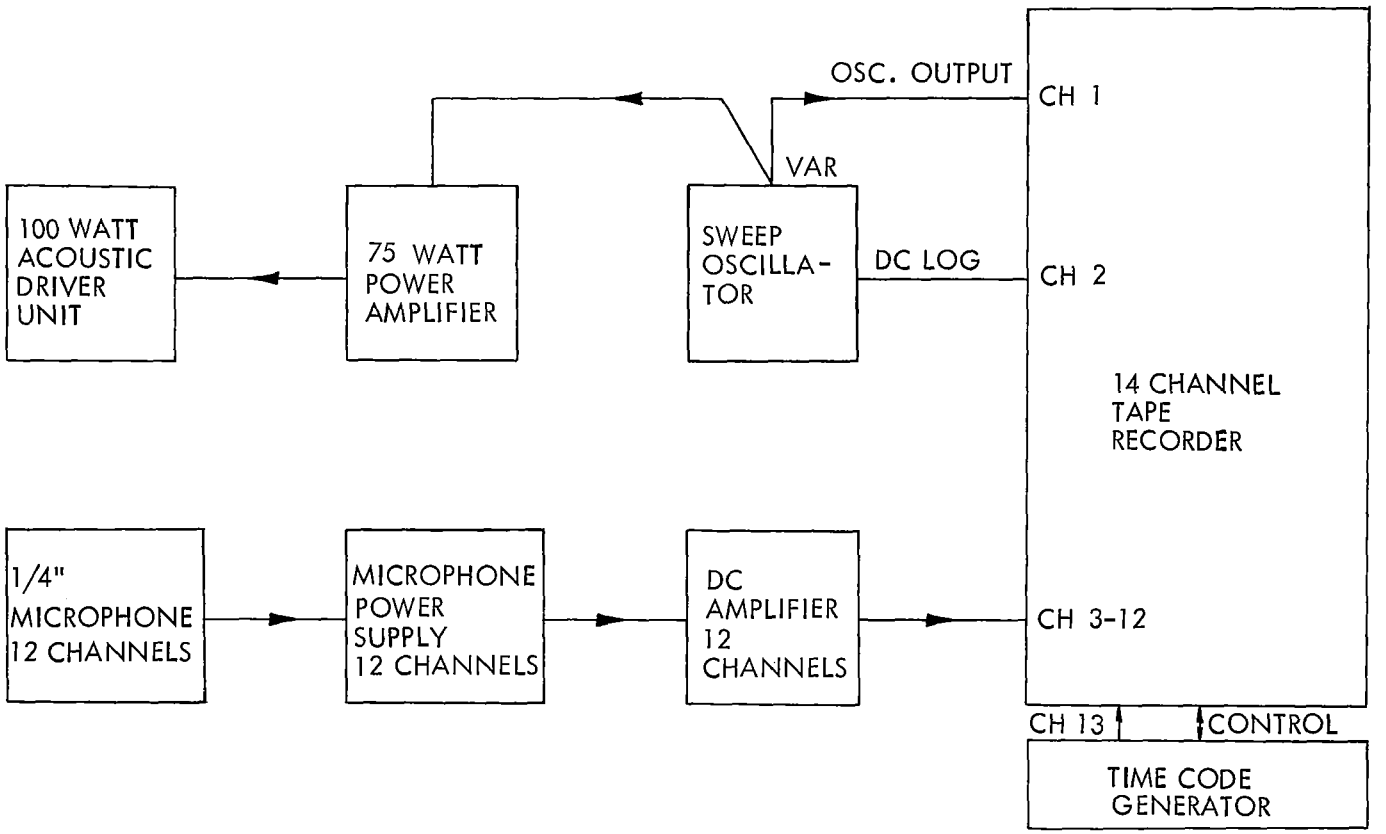

FIGURE 14 INSTRUMENTATION BLOCK DIAGRAM FOR RADIATED PURE TONE DATA ACQUISITION

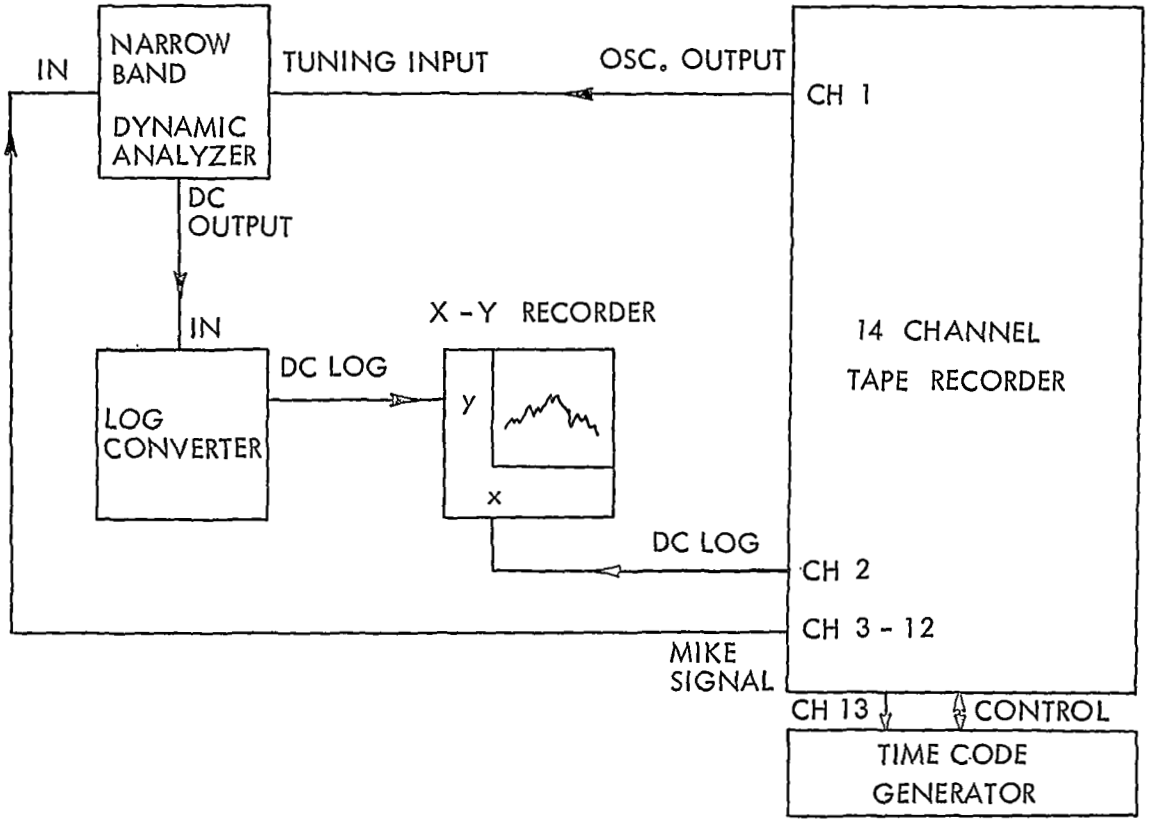

FIGURE 15 INSTRUMENTATION BLOCK DIAGRAM FOR DATA ANALYSIS

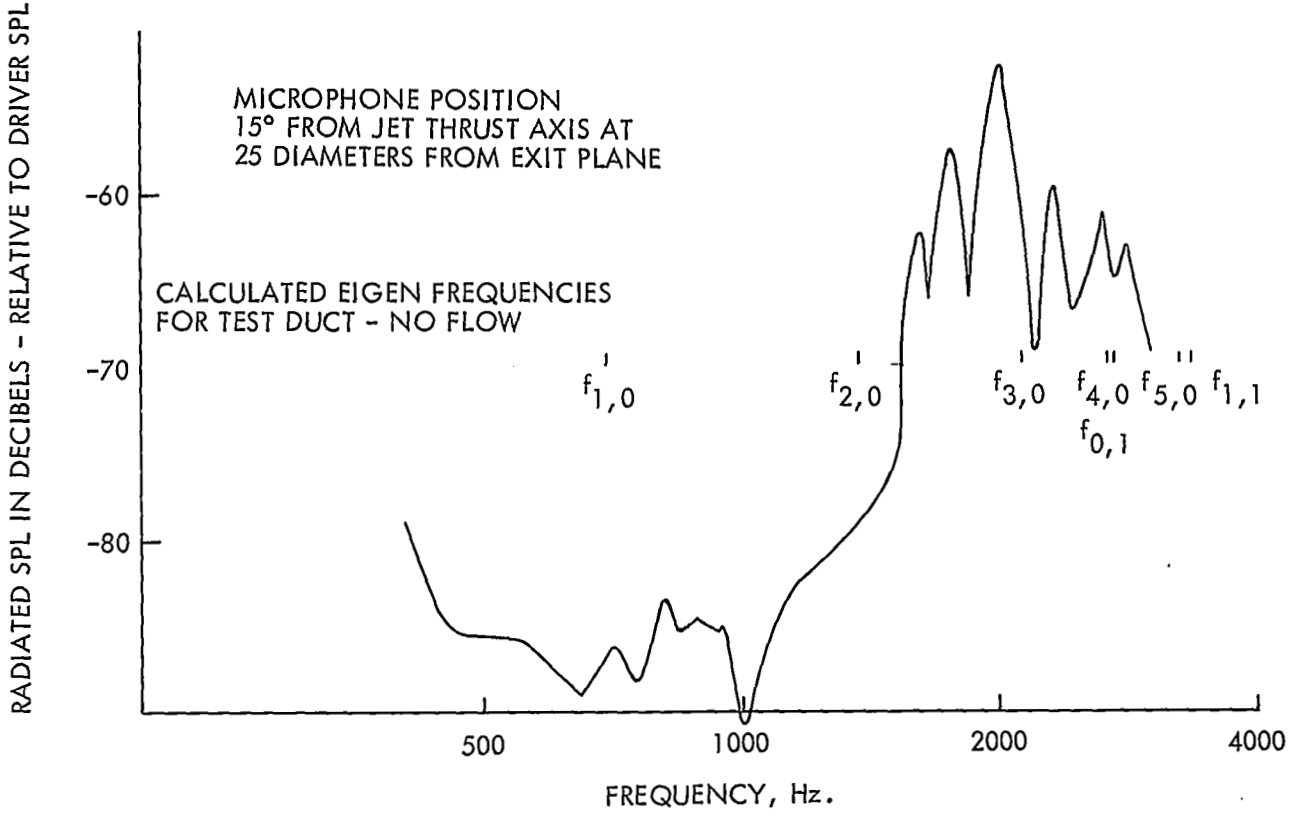

DRIVING PRESSURE PHASED TO EXCITE (2,0) MODE.
NO FLOW - AMBIENT TEMP. CONDITIONS
CALCULATED CUTOFF FREQUENCIES FROM APPENDIX III, SOFRIN & TYLER (REFERENCE 9) FOR HUB TIP RATIO OF 0.5

FIGURE 16 RADIATION RESPONSE OF ANNULAR TEST DUCT

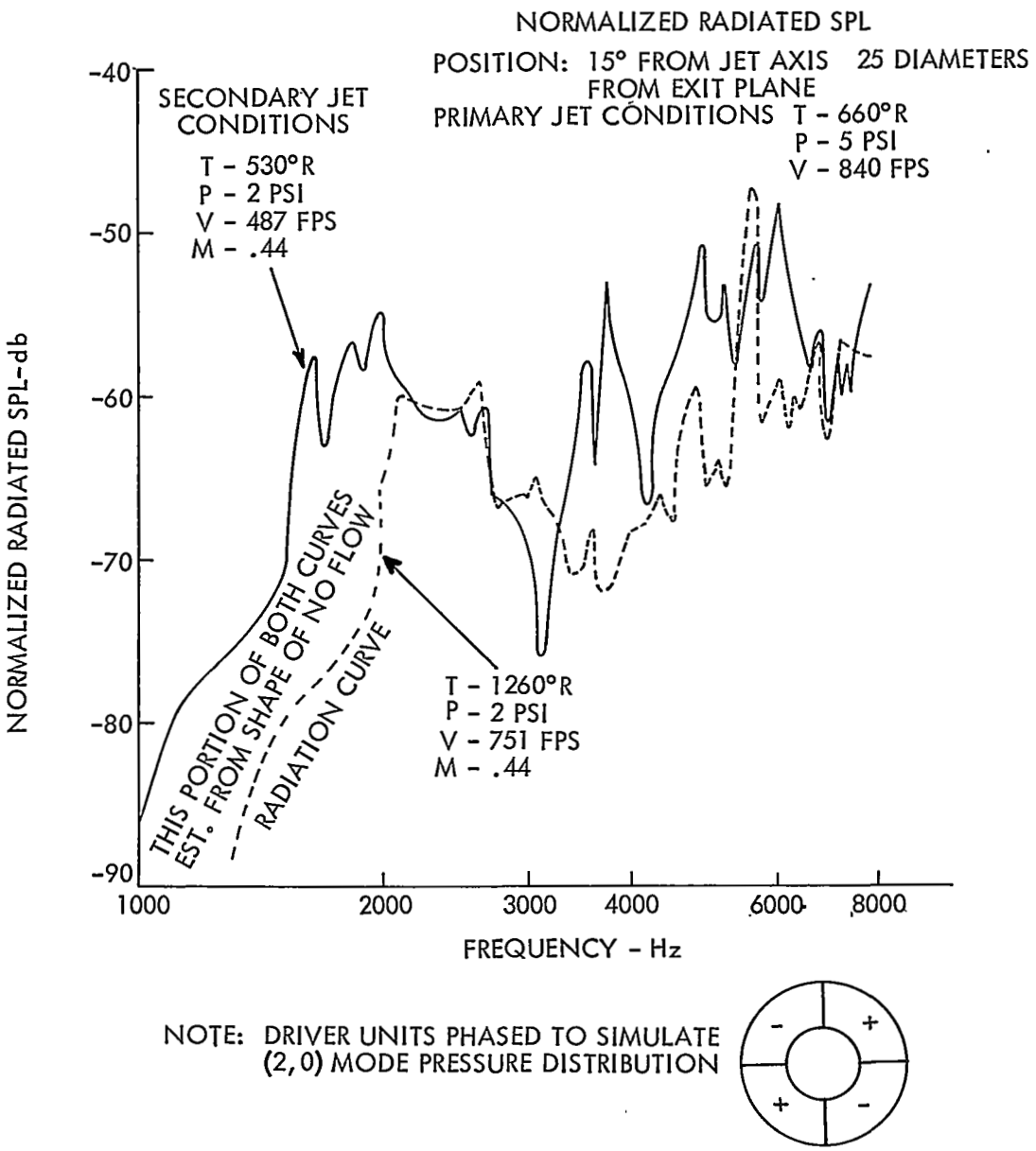

FIGURE 17 RADIATED PURE TONE SOUND PRESSURE SHOWING EFFECT OF TEMPERATURE ON DUCT MODE CUT ON FREQUENCY AND ON LEVEL

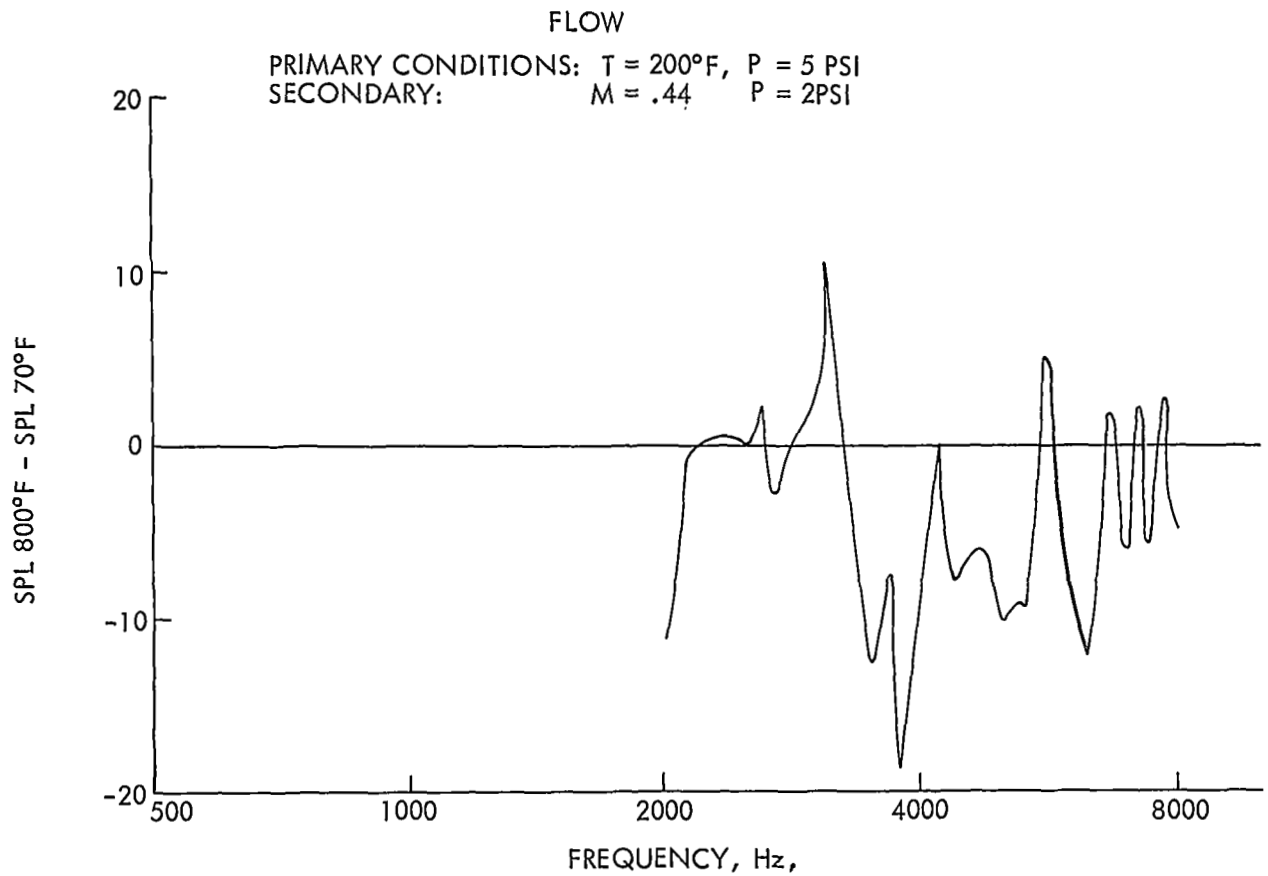

DIFFERENCE BETWEEN RADIATED SOUND PRESSURE LEVEL FOR COLD AND HOT JET WITH SUPERIMPOSED PURE TONE IN (2,0) MODE. MEASUREMENT 15° FROM ℄

FIGURE 18 EFFECT OF TEMPERATURE ON RADIATED PURE TONE SOUND PRESSURE LEVEL - 15° FROM JET THRUST AXIS

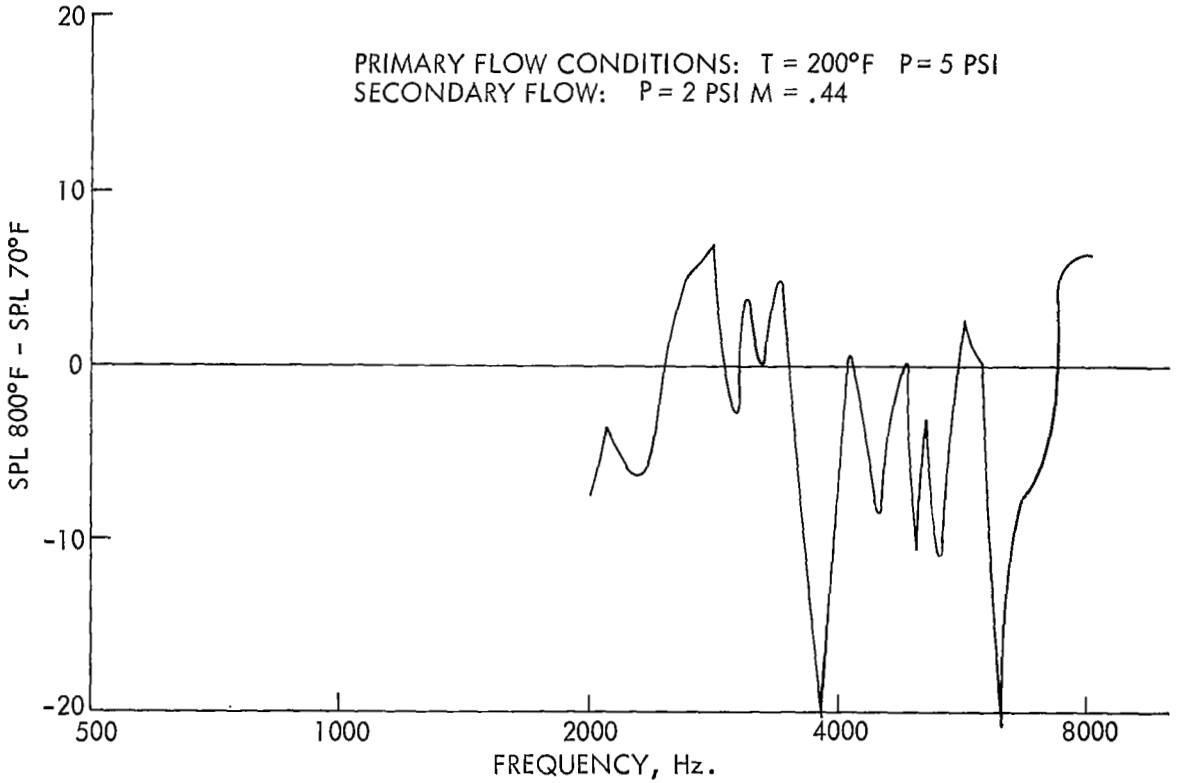

DIFFERENCE BETWEEN RADIATED SOUND PRESSURE LEVEL FOR COLD AND HOT JET WITH SUPERIMPOSED PURE TONE IN (2,0) MODE. MEASUREMENT 45° FROM ℄

FIGURE 19 EFFECT OF TEMPERATURE ON RADIATED PURE TONE SOUND PRESSURE LEVEL - 45° FROM JET THRUST AXIS

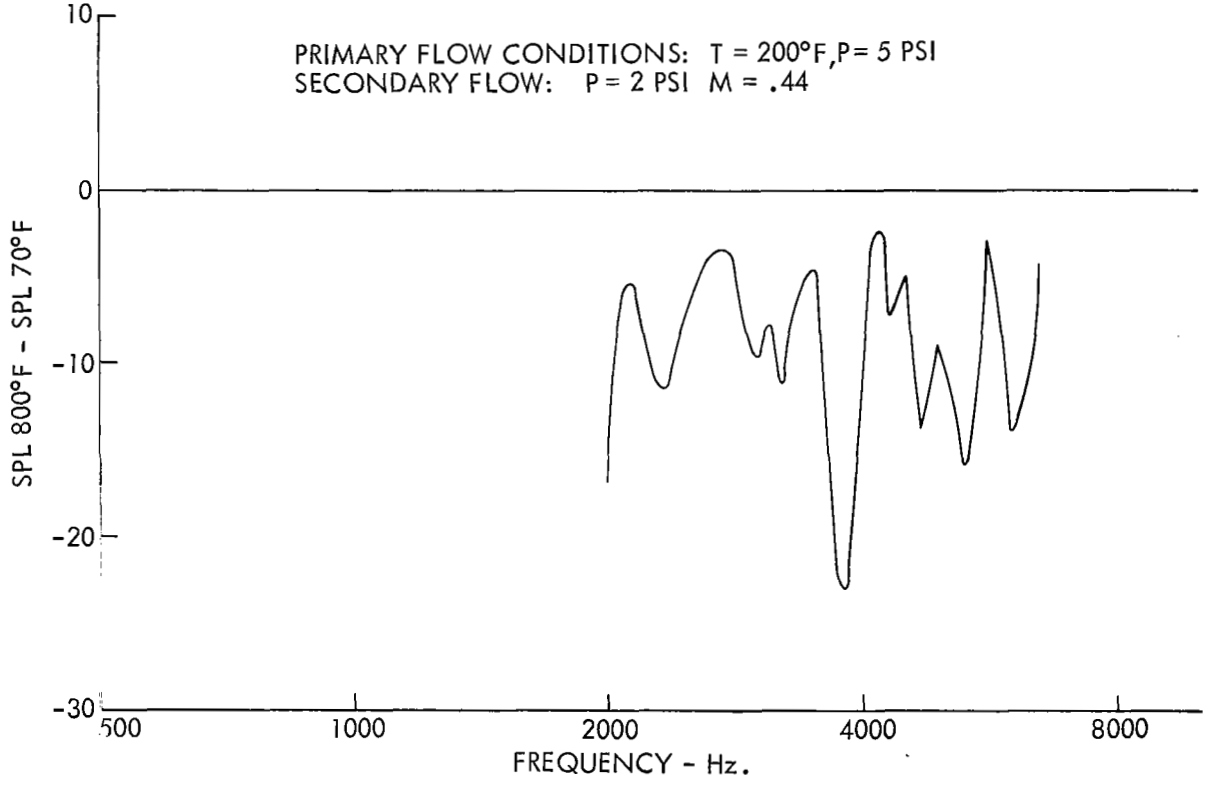

DIFFERENCE BETWEEN RADIATED SOUND PRESSURE LEVEL FOR COLD AND HOT JET WITH SUPERIMPOSED PURE TONE IN (2,0) MODE. MEASUREMENT 90° FROM ℄

FIGURE 20 EFFECT OF TEMPERATURE ON RADIATED PURE TONE SOUND PRESSURE LEVEL - 90° FROM JET THRUST AXIS

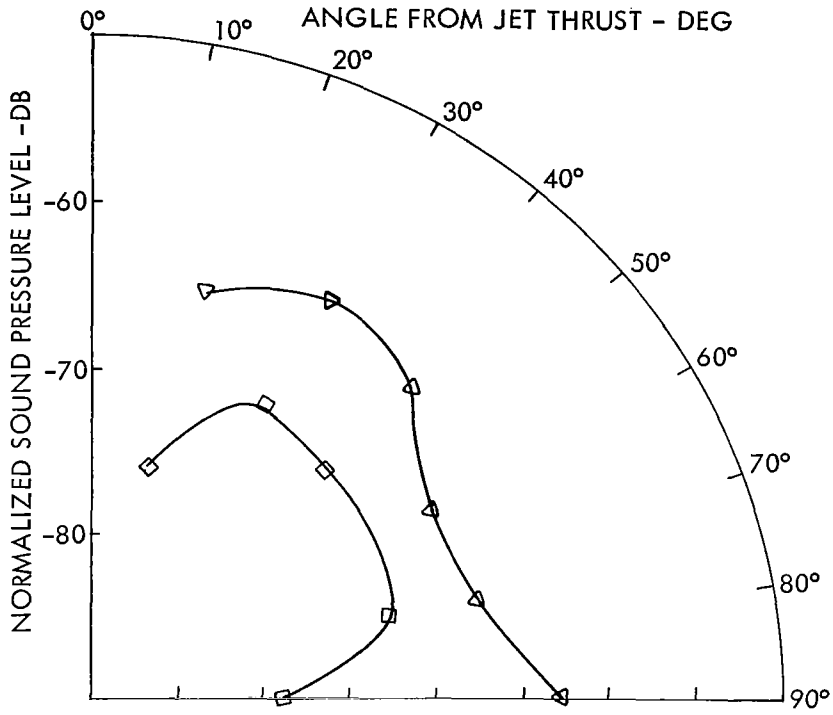

TEST FREQUENCY - 2000 Hz.

DRIVERS PHASED TO SIMULATE (2, 0) MODE
▽ EXIT TEMP - 540°R
□ EXIT TEMP - 1260°R

SECONDARY FLOW CONDITIONS
M = .44

PRIMARY FLOW CONDITIONS
T = 660°R M = .70

FIGURE 21 ILLUSTRATING EFFECT OF JET TEMPERATURE ON PURE TONE DIRECTIVITY - 2000 Hz.

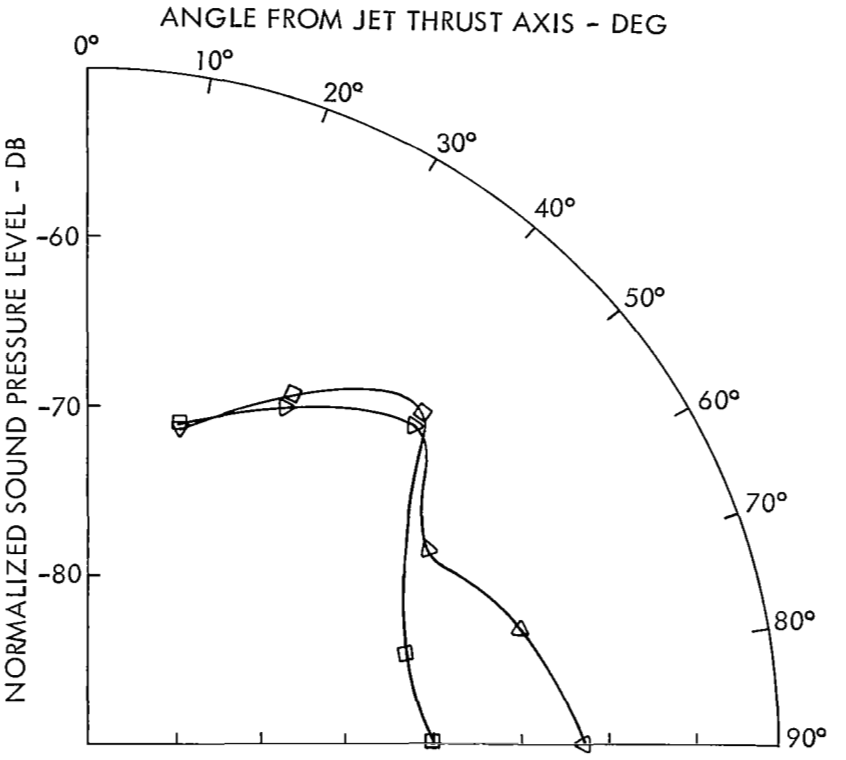

TEST FREQUENCY 2500 Hz

DRIVERS PHASED TO SIMULATE (2, 0) MODE

▽ EXIT TEMP - 540°R

□ EXIT TEMP - 1260°R

SECONDARY FLOW CONDITIONS

M = .44

PRIMARY FLOW CONDITIONS

T = 660°R M = .70

FIGURE 22 ILLUSTRATING EFFECT OF JET TEMPERATURE ON PURE TONE DIRECTIVITY - 2500 Hz

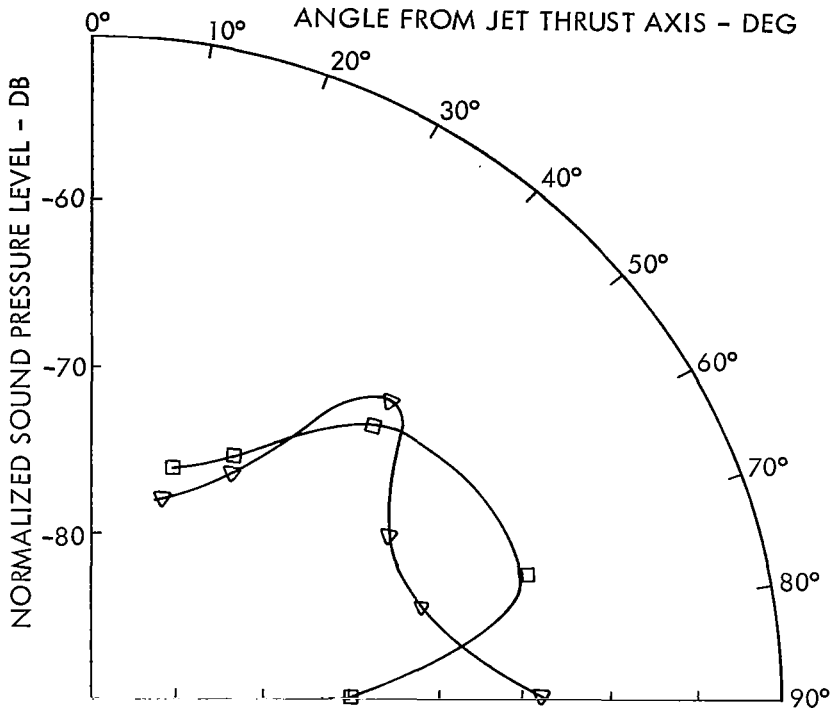

TEST FREQUENCY - 3000 Hz.

DRIVERS PHASED TO SIMULATE (2, 0) MODE
▽ EXIT TEMP - 540°R
□ EXIT TEMP - 1260°R

SECONDARY FLOW CONDITIONS
M = .44

PRIMARY FLOW CONDITIONS
T = 660°R M = .70

FIGURE 23 ILLUSTRATING EFFECT OF JET TEMPERATURE ON PURE TONE DIRECTIVITY - 3000 Hz.

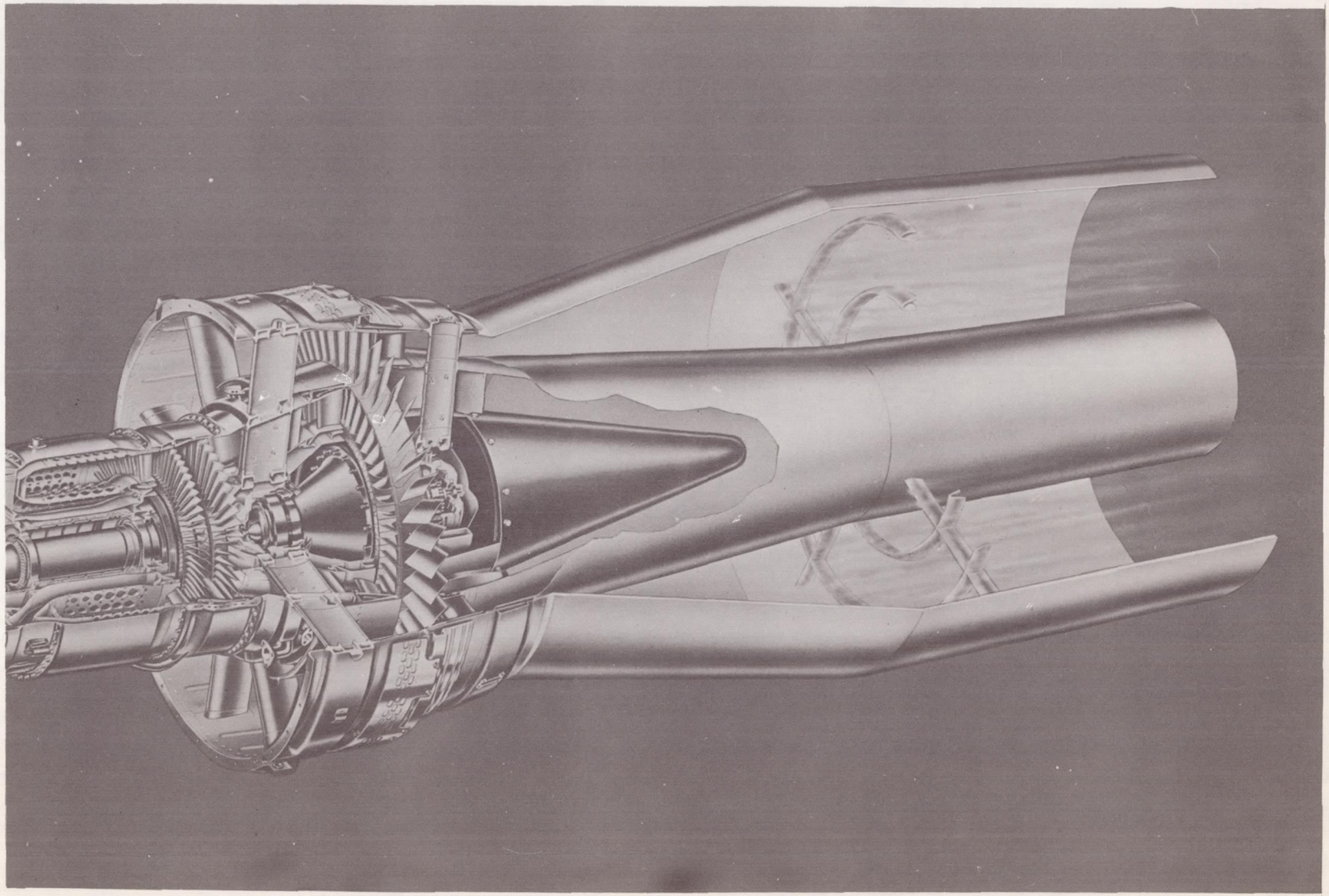

FIGURE 24 ARTISTS CONCEPT OF MODIFICATION NECESSARY FOR EVALUATING JET HEATING ON AN EXISTING ENGINE

APPENDIX A

ENGINE MODIFICATION DESIGN STUDIES

Introduction

The results of analytical design studies for modifying an engine to demonstrate noise reduction through heating are presented here. The purpose of this work was to define and examine the problems likely to arise in modifying a jet engine.

The most promising approach was to attempt a preliminary design for engine modification, which would make the problem areas clearly apparent. So that numerical calculations could be made, as opposed to dealing in sheer generalities, a particular engine was selected for study. Whether this engine, some other engine, or a model is tested, the analysis is applicable; however, the numerical calculations would have to be repeated with different input qualities.

The General Electric CF-700 turbo-fan engine was selected for this analysis since it seemed a promising candidate for future testing. It was the only engine available which satisfied the requirements of low thrust (under 4,000 pounds), availability, and by-pass ratio greater than 1.

Symbols

A	crossectional area
C_p	constant pressure specific heat
D_{ij}	binary diffusion coefficient
L	scale of turbulent intensity
M	molecular weight
m	mass
n	number of moles per unit volume
Q	heat flux
R	gas constant
r	stoichiometric mixture ratio
T	temperature
T*	reduced temperature
t	time
U	gas velocity
V	diffusion velocity
W	mass flow rate

Appendix

x_i	mole fraction of i^{th} species
λ_R	thermal conductivity due to chemical reaction
ρ	density
τ	thrust

Subscripts

a	air
f	fuel
g	gas
o	oxidizer
s	secondary
w	wall
p	primary

Combustion Chamber Geometry

Chamber Diameter.- From available manufacturers, information on the CF-700, the following values of effective exhaust velocity of the primary U_p, effective exhaust velocity of the secondary U_s, bypass ratio, primary exhaust gas temperature T_p, secondary exhaust gas temperature, T_s, and thrust, τ , were used to calculate the chamber diameter:

$$\begin{aligned} U_p &= 1600 \text{ ft/sec} \\ U_s &= 800 \text{ ft/sec} \\ T_p &= 1000°F \\ T_s &= 200°F \\ \tau &= 4000 \text{ lb F} \end{aligned} \qquad \text{(A-1)}$$

It was assumed that all the diffusion of the secondary air would take place prior to burning. In most practical situations, the secondary air may travel a fairly long distance from the fan to the exit plane, so this distance is available for diffusion. Since the same amount of diffusion must take place whether it is done before or after burning, it might just as well be done before burning, for it is considerably easier to work with cold air rather than very hot air.

The chamber diameter will, therefore, be assumed such that the secondary air velocity after burning will be 800 ft/sec. Since the bypass ratio and thrust are known, the following equations may be solved for the primary and secondary mass flow rates:

$$\frac{\dot{W}s}{\dot{W}p} = 2 \qquad \frac{\dot{W}s(Us)}{g} + \frac{\dot{W}p(Up)}{g} = \tau(A\text{-}2) \qquad (A\text{-}2)$$

Therefore, using the values given in equation (A-1),

$$\dot{W}p = 41 \text{ lb m/sec} \qquad \dot{W}s = 82 \text{ lb m/sec}$$

From the equation of state

$$\rho = \frac{P}{RT} \qquad (A\text{-}3)$$

the density of the primary and secondary exhaust gases may be determined, and finally the area of the primary and secondary exhaust may be calculated using the continuity equation

giving $\dot{W} = \rho AU$

$A_p = 136.8$ sq in

$A_s = 246$ sq in

Assume the secondary exhaust gas temperature after burning to be 2500°R. This is a reasonable upper bound for several reasons. To conduct acoustical tests of the effect of secondary exhaust heating without effects of other unwanted changes, the primary and secondary streams are to be separated by a partition (see figure 24). Because of its location, cooling would be very difficult, and 2500°R is a reasonable limit for materials from which this partition could be made. (It should be noted, however, that advanced jet engines have been designed with exhaust gas temperatures up to 4000°R, using some rather exotic cooling techniques.)

Since the temperature with burning is now fixed at about 3.6 times the temperature without burning and the velocity is to remain constant, the continuity equation requires that the secondary area increase by a factor of 3.6. Thus

$$A_s = (3.6)\ (246) = 895 \text{ sq in}$$

Therefore, the outside diameter is approximately 36 inches. This is also just about the limit of the engine nacelle envelope.

Chamber length.- Rough calculations demonstrated that, if the chamber were made long enough to allow the flame to propagate radially to within a short distance from the wall, it would be sufficiently long to allow liquid drops (of a size that would be produced by any reasonable atomization of the fuel) to burn completely before leaving the chamber. Therefore, flame - spreading rather than liquid - droplet burning determines the chamber length. Although it is possible to perform theoretical calculations for the rate of flame - spreading, this area is not well enough developed to place confidence in calculations based on existing theories (ref.11, for example) over engineering judgement based on experimental results.

The chamber length chosen was based on reference 12 and the assumption that, since the chamber entrance velocity reported was approximately three times the entrance velocity for this study (determined already since the chamber diameter has been specified), then a chamber length of approximately one-third that of reference 12 should be about right. Some additional length was added because the air entering the afterburner discussed in reference 12 is much hotter than that in this study and would tend to accelerate effects such as chemical kinetics vaporization.

Aerodynamincs

Two aerodynamic problems were studied in this investigation. Vortex shedding from the flameholders was examined because it was first thought that this was an important phenomenon associated with combustion instability. However, further study of the available literature indicated this is not the case.

The only anticipated major aerodynamic problem involved diffuser design. Unless screens or vanes or some other mechanism is used, the flow will separate if the equivalent conical expansion angle is greater than about 8°. A diffuser with an equivalent conical expansion angle of less than 8° for the area ratio required in this report (3.6) would be extremely long. Consequently it is reasonable to assume that, in any practical application of jet heating, a wide-angle diffuser would be used, with a device such as vanes, screens, or suction, to prevent separation. Determining the practicality of using duct burning on existing engines is not the prime purpose of this investigation. However, certain facts which have a bearing on feasibility have been considered because any modified test engine should resemble flight hardware to the extent that both will have similar acoustic properties.

A model of the modified engine fan duct was built (see figure 25). The center body and outer casing of the annular diffuser was made up of 3/4 inch sections so that screens could be inserted easily at a variety of locations.

The model diffuser and combustion chamber was run first without screens but with the exhaust nozzle. A large loss in total pressure was observed. The nozzle and combustion chamber were removed, and the flow distribution was observed. The flow was found to separate nonsymmetrically. With the insertion of a single screen, the flow still separated from the walls, but symmetrically. Crude estimates of the pressure-drop coefficient for several different screens were obtained from measurements. They were compared with those predicted by charts and nomograms in references 13 and 14, with very poor agreement. It was suspected that the Reynolds numbers for the runs being made were outside the range of the charts and nomograms being used to predict the pressure-drop coefficients. Samples of the screens were placed between two straight pieces of pipe, and the pressure drop coefficient was measured for Reynolds numbers over the range of interest. The results are shown in figure 26. Following the method outlined in reference 13, screens were now selected

and placed in the diffuser making the best choice between screens available and discrete locations available for inserting them. The resulting arrangement was then tested and found to perform satisfactorily.

Fuel Injection, Vaporization and Ignition

The overall air-fuel ratio at which the burner is to be run is quite lean. To keep the flame attached to the flameholder (see the section on burning), it is necessary to have a nearly stoichiometric mixture in the neighborhood of the flameholder. Consequently, it would be necessary to concentrate the fuel in the neighborhood of the flameholder by injecting fuel into the air stream judiciously. Therefore, the problem of air fuel mixing was studied.

The most promising analytical approach to the problem, (as reported in reference 15) seemed to be a theory of turbulent mixing proposed by G. I. Taylor. A computer program based on this theory was written to predict the fuel-air ratio downstream of a distribution of point sources of fuel injected into an air stream. A report (ref. 12) giving sufficient details of experimental work to provide verification for theoretical calculations was very useful. To test the validity of the program, calculations were made for the fuel injection system of reference 12. The results are shown in figure 27. The flow in the diffuser shown was visualized as potential flow with turbulent mixing superimposed so that a stream tube surrounding each injector hole was taken as the duct of infinite diameter in the analysis. The stream tube centers were located downstream using dimensions from reference 12. As suggested in the literature and to perform the calculations, the scale of the turbulence L was taken as .17 times the diffuser diameter, and the intensity $\sqrt{\overline{\mu^2}}$ was taken as 3% of the main stream velocity.

Although the theoretical calculations performed agree well with experimental results, the theoretical considerations cannot be completely relied upon; they should be used more for qualitative rather than quantitative information. Based on the analytical work done, it appears that if a liquid fuel is to be used, the spray bars must be located fairly well upstream to ensure good atomization and sufficient vaporization. This suggests that a flameholder for the conditions of this study for liquid fuel should have no more than about two or three concentric rings; otherwise, the difficulty of controlling the fuel-air ratio in the neighborhood of the flameholder would be too great. If a vapor fuel were to be used, as would possibly be done if a small model were built to test the acoustical concepts, this limitation would not apply, since spray bar and flameholder could be as closely coupled as necessary.

Preheating the liquid fuel was considered as a method of conveniently controlling the vaporization. Although it was expected that preheating the fuel from 70°F to 200°F would vary the vaporization rate over quite a range, the effect on vaporization of preheating the fuel up to a temperature of 200°F was found to be quite small. Preheating to higher temperatures was not considered because of undesirable side effects such as cracking and coking of the fuel and the possibility of creating a fire hazard.

Spark ignition will probably be chosen, since this system is the most convenient of all systems currently used. Although reference 16 indicated difficulty in igniting cold kerosene this difficulty can probably be eliminated.

Appendix

Assuming the mixture requiring the minimum ignition energy to be that which results in the highest central temperature in the small volume containing the spark, the following approximation can be used to determine the optimum mixture ratio

$$m_f/m_o = (D_o/D_f)^{1/2} r \qquad \text{(A-4)}$$

where
- r = stoichiometric mixture ratio
- D_o = diffusivity of oxidizer
- D_f = diffusivity of fuel

Since the curves of minimum energy for ignition versus mixture ratio are quite steep, it will be necessary to have a mixture ratio, in the neighborhood of the igniter, close to the optimum mixture ratio as calculated by equation (A-4). For the application being considered, this will create a requirement for either a ducting of the fuel and a portion of the air to achieve the desired mixture ratio in the ignition region, or a higher than normal fuel injection rate on starting. The second approach represents the simplest solution to this problem.

While the mechanisms of spark ignition cannot be completely explained theoretically, a large volume experimental data is available in references 17 through 20 to facilitate the design.

Burning

Two topics were considered in connection with the burning process: flame stabilization and combustion chamber length. A bluff-body flame stabilization system was chosen, not because it is better than all other systems, but because it is the most common system and therefore easier to deal with. (An opposed jet flame stabilization system, for example, could involve a separate research project, quite beyond the scope or intent of this study.)

Once a bluff-body flame stabilization system had been decided upon, the question of flameholder width quite naturally arose. All the literature surveyed was in agreement that, for efficient burning, the flameholder system should be built of concentric rings of minimum width necessary to hold the flame, and should present approximately 30% blockage area to the air stream. This is most clearly explained in reference 16. Several workers assert that combustors with smaller-width flameholders are less likely to exhibit combustion instability (see reference 21, for example).

Data on the blow-off limits for bluff body flameholders operating very near the conditions of this study were found in reference 22. Figure 29 is a graph taken from reference 22, showing blow-off limits for cylinders of various sizes. The fuel for which this graph was drawn is somewhat more volatile than the usual aviation fuels, such as JP4, JP5 and kerosene, but similar in all other respects. Note that there is a 150°F to 200°F temperature rise through the fan stage of the CF-700 fan jet engine, which places the temperatures close together as well. Figure 28 shows the adiabatic flame temperature for JP4 and 200°F air for various equivalence ratios. Since a temperature after burning of 2500°R is desired, the overall equivalence ratio would be around .404, as shown in figure 28.

The point corresponding to an equivalence ratio of .404 and a velocity of 200 ft/sec lies far outside the envelope of all the curves of figure 29. This means that operation at

this condition would be impossible with a uniformly mixed gaseous fuel air combination without using a flameholder of rather large dimensions. The problem car be overcome by designing the fuel injection system so that approximately a stoichiometric mixutre ratio will be obtained locally in the neighborhood of the flameholder. What will ultimately determine the width of the flameholder is not so much blow-off limits directly, but the fact that there is a practical limit on the width of the flameholder below which it would be extremely difficult to design a fuel injection system that would maintain a locally rich enough mixture in the neighborhood of the flameholder. Factors associated with liquid fuel assist in enriching the mixture around the flameholder. For example, the unvaporized droplets carried by the gas stream flowing toward a flameholder are heavy and will not follow the gas stream as it flows around the flameholder but rather will continue in a straight path and strike the hot flameholder, vaporize, and locally enrich the mixture. A flameholder design incorporating the ideas of this section and the previous section is shown in figure 30.

Heat Transfer

Two separate approaches were taken in estimating the heat transfer. The first method follows references 23 and 24. For the calculations made by this method, the most extreme operating conditions that might reasonably be expected to occur were assumed. A cooling system was designed on the basis of these calculations, since it was thought desirable that it should be capable of providing adequate cooling under the most adverse conditions that might arise. Calculations based on a second entirely different approach were also made. The assumptions made were a little less drastic, to provide a verification of the first calculations and to provide more realistic estimates of heat transfer under normal operating conditions.

Assume the gas temperature, T_g, to be 3500°R and the gas velocity, V_g, to be 800 ft/sec and a wall temperature, T_w, of 500°R. While 3500°R is not the maximum temperature theoretically possible, it is an estimate of what might be expected under adverse conditions resulting from uneven fuel distribution, for example. The density, ρ , the constant pressure specific heat, C_p, and the molar rate of change of each species with temperature $\partial x_i/\partial T$ were found by using a combustion program assuming JP-4 and 200°F air in a mixture ratio to give an adiabatic flame temperature of 3500°R. The calculated values are,

$$C_p = .3554 \text{ BTU/lb m } ^\circ\text{R}$$

$$\rho = .0112 \text{ lb m/ft}^3$$

According to reference 22, the thermal conductivity due to chemical reaction may be estimated from

$$\lambda_R \frac{dT}{dz} = \sum_i g_i H_i \qquad \text{(A-5)}$$

where

$$g_i = n x_i V_i \qquad \text{(A-6)}$$

and n is the number of moles of the gas mixture per cm^3, V_i is the diffusion velocity of molecules of the ith kind and H_i is the enthalpy of the ith species per mole.

Appendix

By using the methods outlined in reference 24, values of the transport properties were found and subsequently used in a Nusselt-type experimental heat-transfer correlation to obtain an estimated heat flux.

$$Q/A = 84.3 \text{ BTU/Sec ft}^2$$

A separate analysis based on the boundary-layer theory of reference 25 gave the results shown in figure 31. These more nearly approximate the heat transfer to be expected under normal operating conditions.

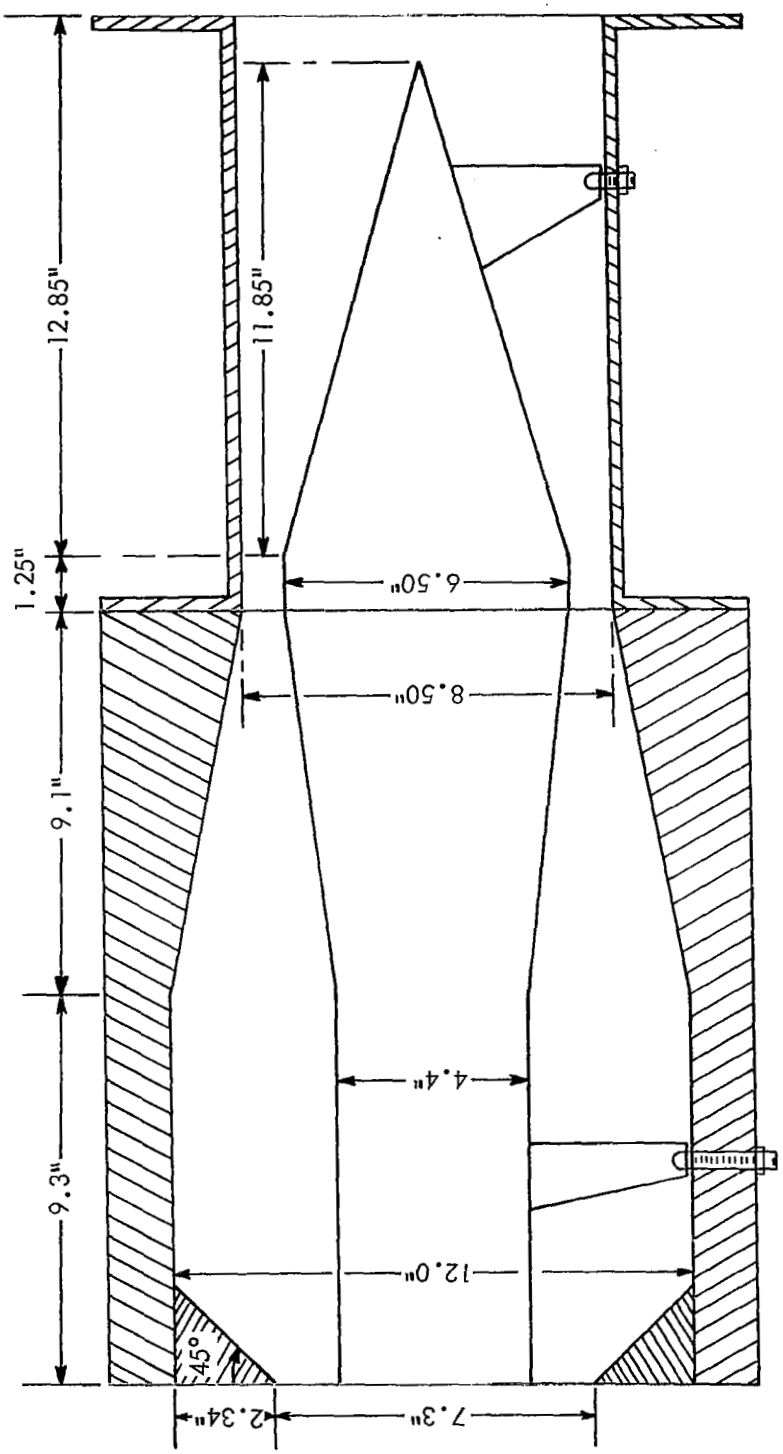

FIGURE 25 DIFFUSER MODEL ARRANGEMENT

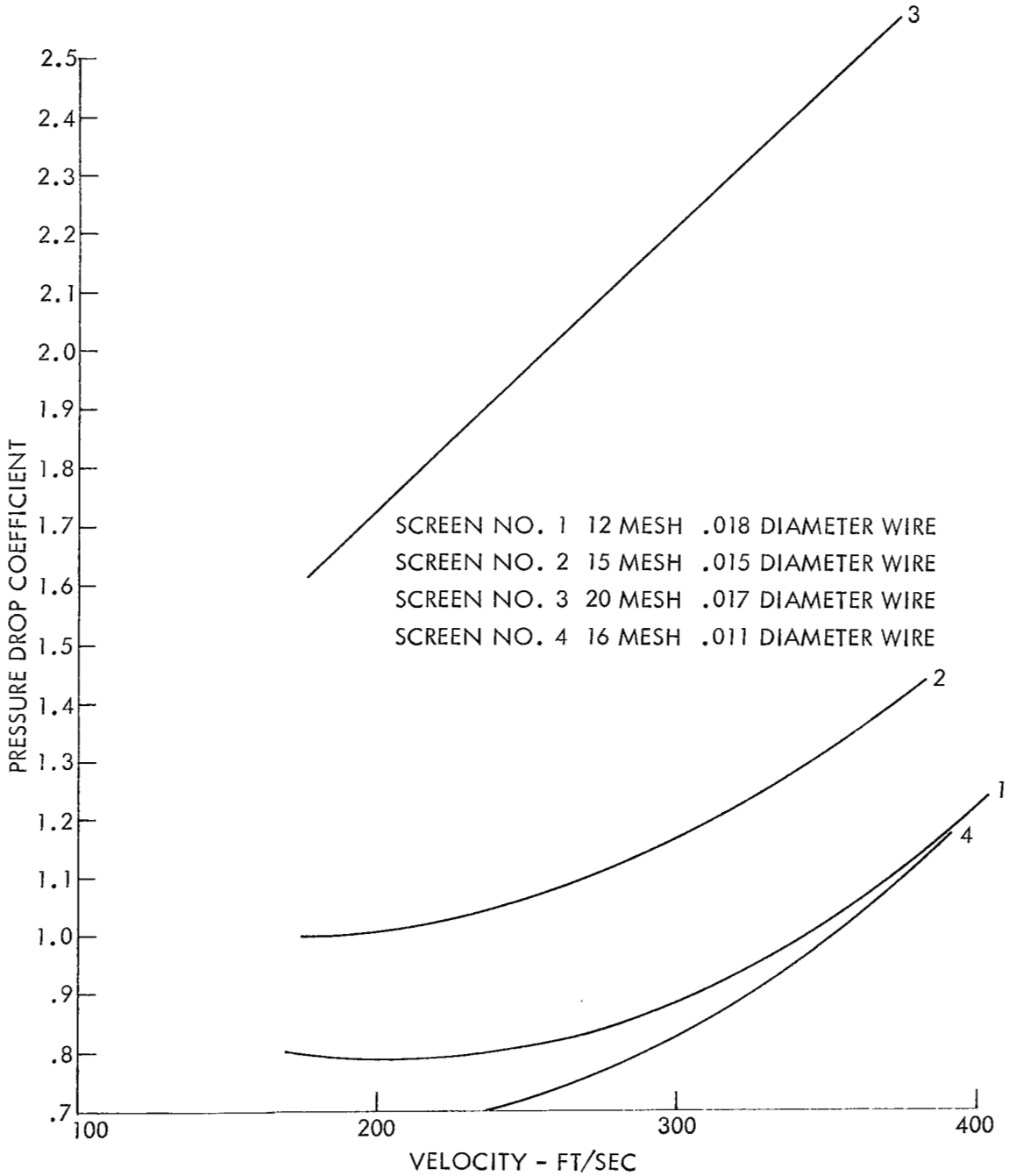

FIGURE 26 PRESSURE DROP COEFFICIENTS FOR SCREENS TESTED VS. VELOCITY UP STREAM OF SCREEN

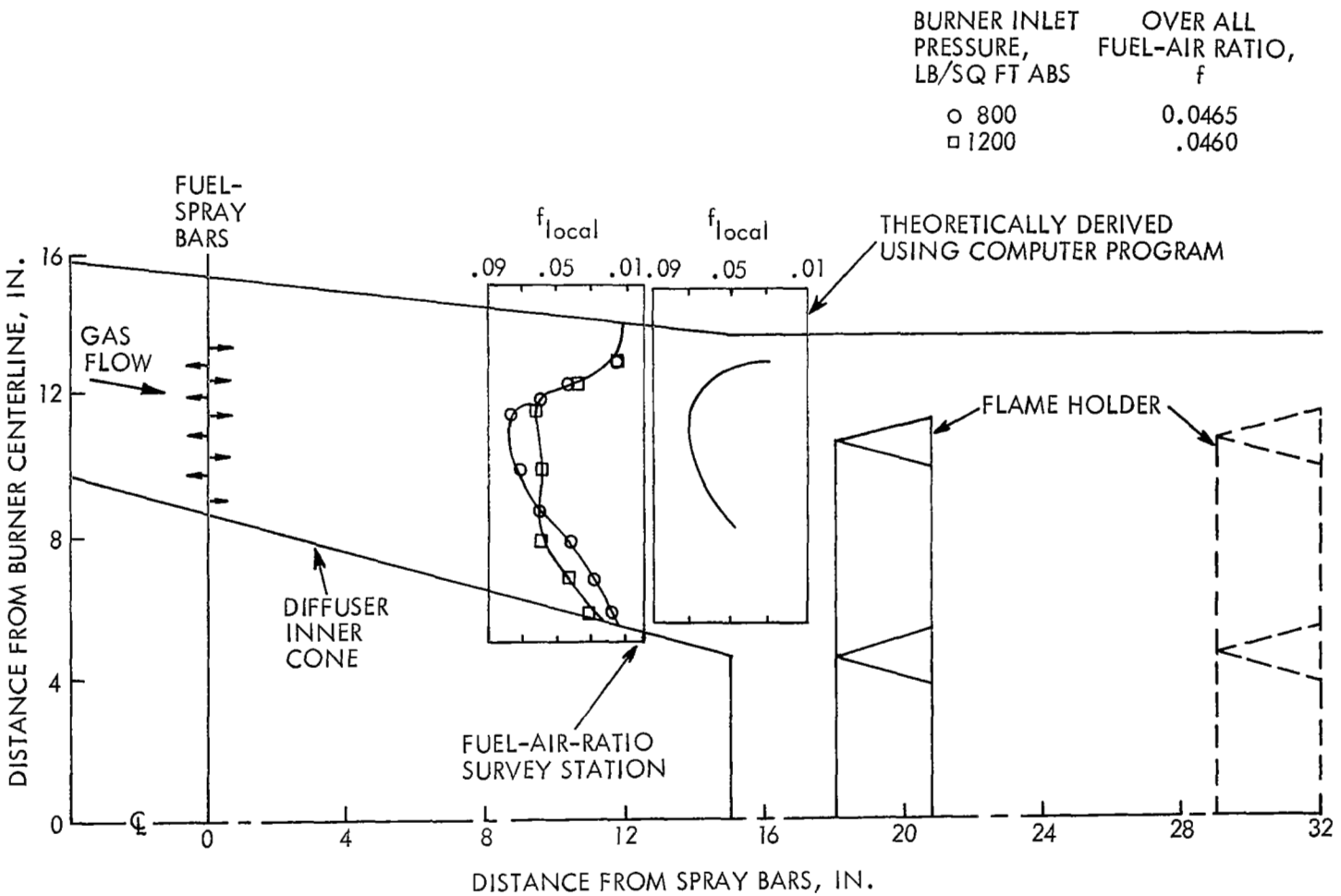

FIGURE 27 EFFECT OF BURNER-INLET PRESSURE ON FUEL-AIR RATIO. RATED ENGINE OPERATION. (FROM REFERENCE 12, EXCEPT FOR THEORETICAL CALCULATION)

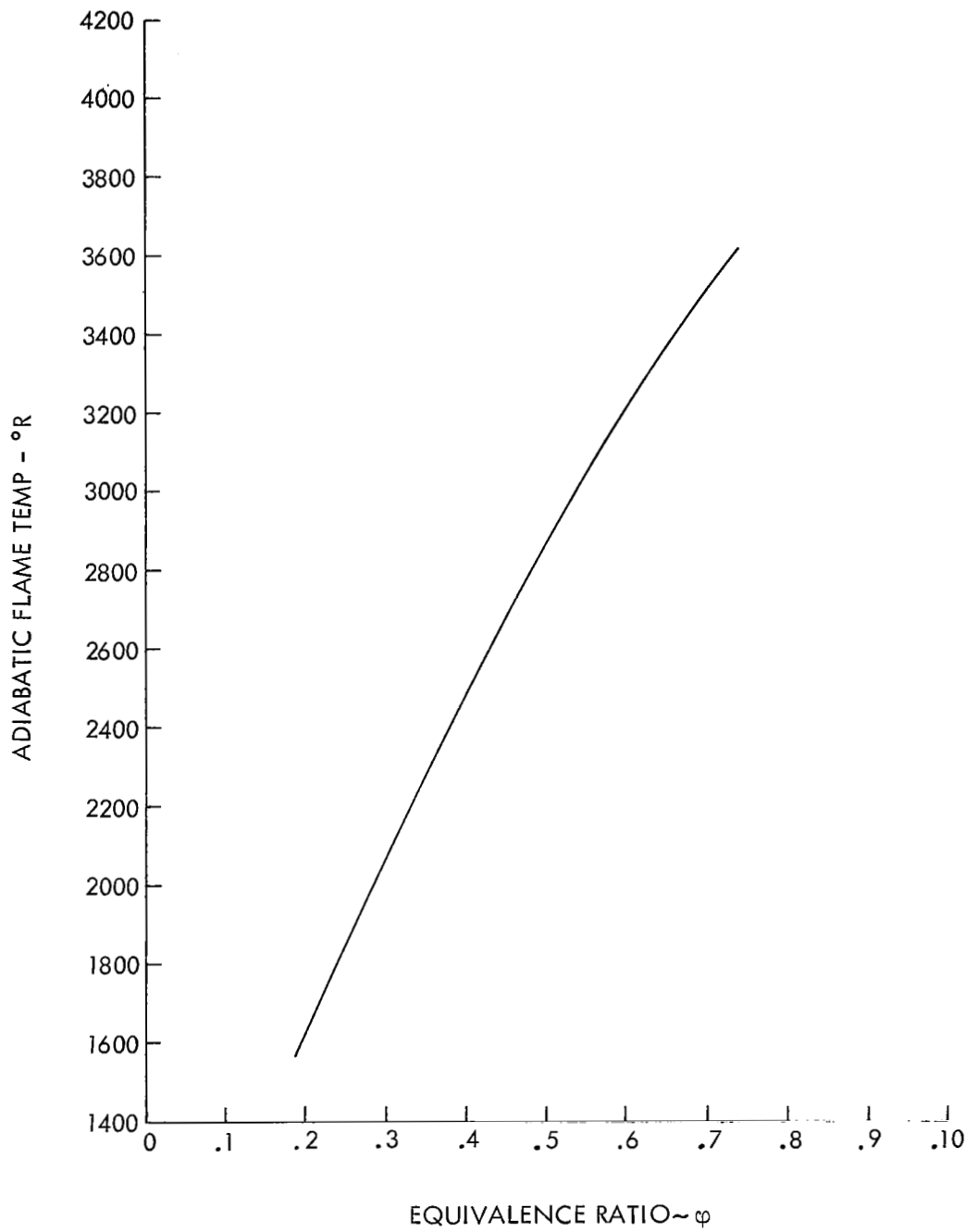

FIGURE 28 ADIABATIC FLAME TEMPERATURE FOR JP-4 AND AIR - 200°F VS EQUIVALENCE RATIO

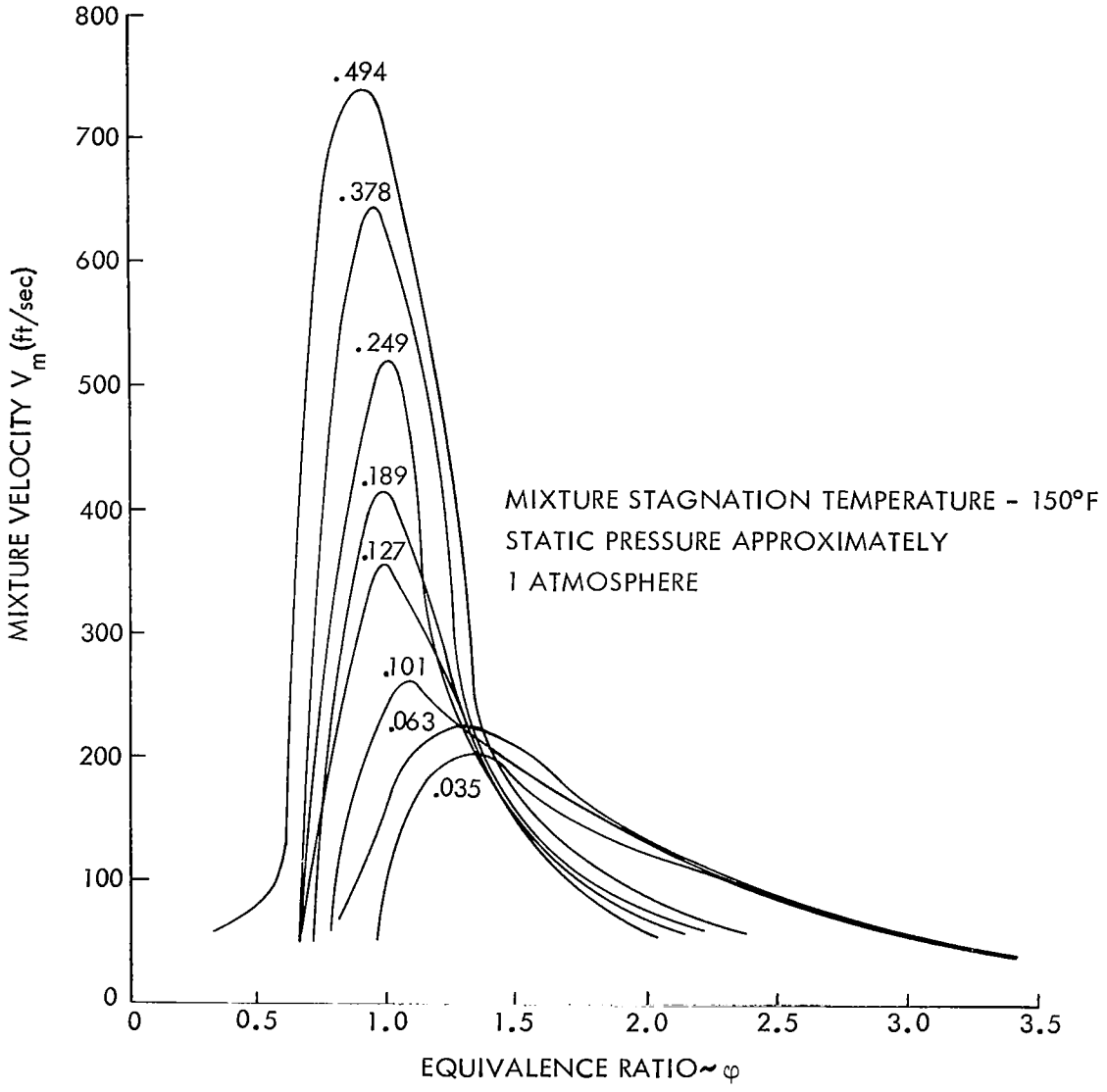

FIGURE 29 FLAME BLOWOFF LIMITS FOR CYLINDER SIZES FROM 0.035 TO 0.494 INCH IN DIAMETER (FROM REFERENCE 22)

$D = 13.2''$
$R_1 = 8.6''$
$R_2 = 9.6''$
$R_3 = 11.33''$
$R_4 = 12.33''$
$R_5 = 14.1''$
$R_6 = 15.1''$
$R_7 = 18''$

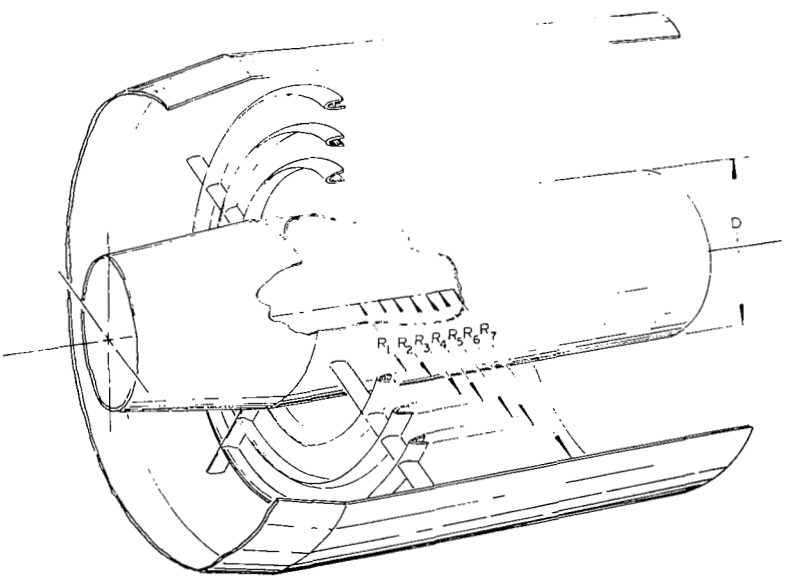

FIGURE 30 PROPOSED FLAME HOLDER DESIGN FOR STUDY MODIFICATION

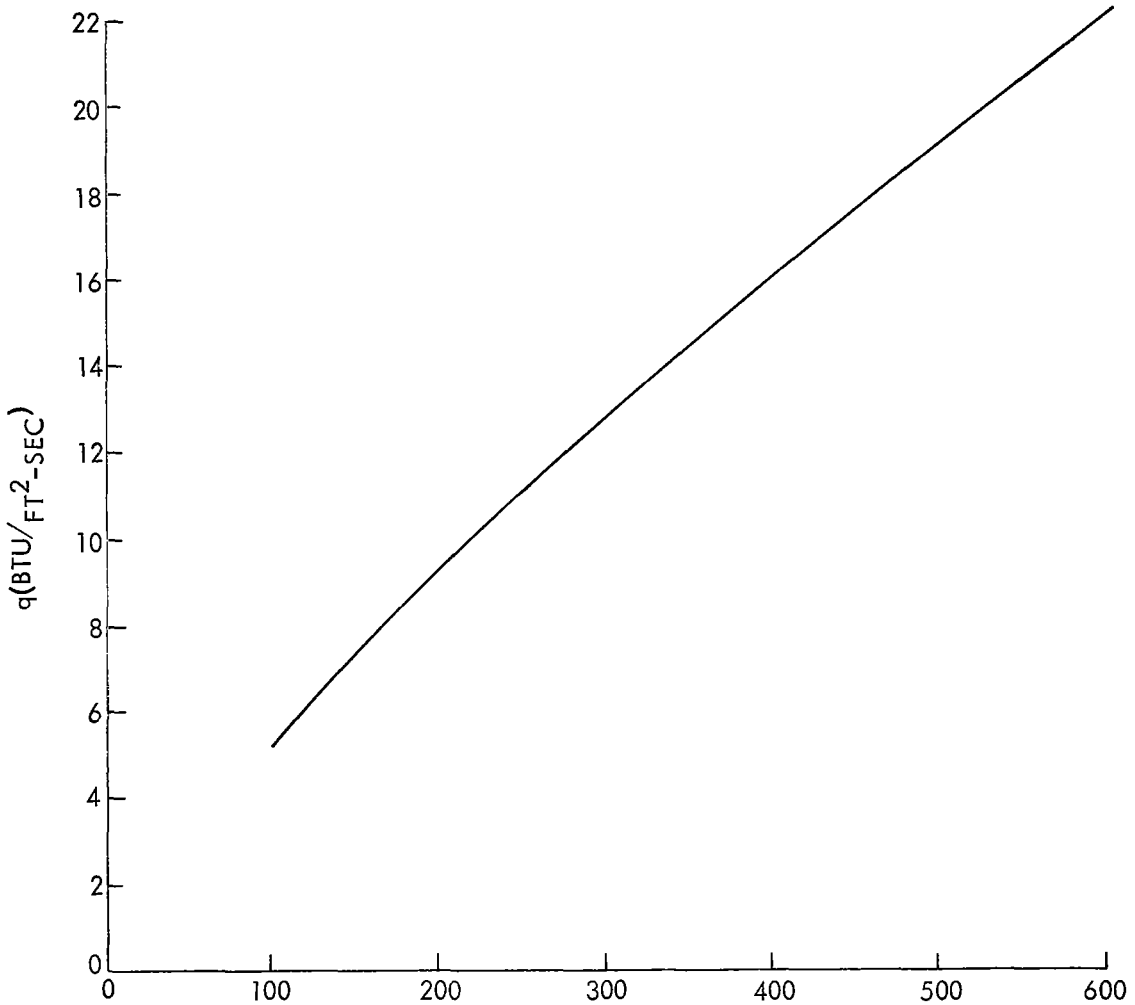

FIGURE 31 HEAT TRANSFER THROUGH 1000°R DUCT WALL

APPENDIX B

THEORETICAL ANALYSIS OF COMBUSTION INSTABILITY IN AN ANNULAR AFTERBURNER

Ben T. Zinn*

Introduction

In studies of combustion oscillations, it is customary to use the frequency of the oscillations as a means of distinguishing among various types of combustion instability. During low-frequency oscillations, the gas in the combustor oscillates in unison, and the pressure oscillations have no spatial dependence. Intermediate-frequency instability is considered to be associated with mixture-ratio oscillations. This type of instability is seldom observed. High-frequency combustion instability occurs when one of the natural acoustic modes of the combustor is excited. The high-frequency instability is the most detrimental and least understood type of combustion oscillations. Unless detected in time, the presence of high-frequency combustion oscillations is bound to result in the complete destruction of the propulsive device. It is the elimination of this type of instability that the analysis presented herein will be primarily concerned with.

Symbols

c	velocity of sound
C_v	specific heat at constant volume
f_o	quantity defined in eq. (B-30)
i	imaginary unit
$k(r, \theta, t)$	quantity defined in eq. (B-19)
L	combustor length
p	pressure
P, R, S, U, V, W	z dependant variables defined in eq. (B-18)
Q_E	energy source
Q_M	mass source
r	radial length
$S^{\sigma}(n,q)$	root of eq. (B-36)
s	entropy
t	time
u, v, w	axial, radial and tangential components of velocity perturbations
Y	complex number defined in eq. B-38

*Associate Professor, School of Aerospace Engineering, Georgia Institute of Technology.

γ	ratio of specific heats
ζ, π, τ	quantities defined in eq. (B-17)
Θ	quantity defined in eq. (B-34)
θ	tangential coordinate
λ	amplification factor
ρ	density
ψ	solution of Bessel equation (see eq. (B-35))
ω	frequency of pressure oscillations
$\underset{\rightarrow}{\nabla}$	gradient operator

Subscripts

$(\ )_o$	quantity evaluated at the combustor entrance (i.e., z = 0)
$(\ )_r$	reference quantity

Superscripts

$(\ )^*$	dimensional quantity
$(\bar{\ })$	steady state quantity
$(\ )'$	perturbed quantity

Derivation of Equations

Due to the complexity of the flow field in the combustor and due to our limited ability to describe this flow field analytically, it becomes necessary to consider a theoretical model that closely resembles the actual flow field and at the same time is amenable to an analytical solution. Neglecting the fuel mass addition (which is a reasonable assumption for an air-breathing propulsion system) and assuming the gas in the combustor to be inviscid, nonheat-conducting, and to behave as a calorically perfect gas, then the nondimensional conservation equations which describe this flow can be expressed in the following form:

$$\frac{\partial \rho}{\partial t} + \nabla \cdot (\rho \underset{\rightarrow}{u}) = 0 \tag{B-1}$$

$$\frac{\partial \vec{u}}{\partial t} + (\underset{\rightarrow}{u} \cdot \underset{\rightarrow}{\nabla})\underset{\rightarrow}{u} + \frac{1}{\gamma \rho} \nabla p = 0 \tag{B-2}$$

$$\frac{\partial s}{\partial t} + (\underset{\rightarrow}{u} \cdot \underset{\rightarrow}{\nabla}) S = \frac{Q}{p} \tag{B-3}$$

$$s - s_r = \ell n\, p - \gamma\, \ell n\, \rho \tag{B-4}$$

where

$$\rho = \frac{\rho^*}{\rho_r^*} \quad , \quad \underset{\rightarrow}{u} = \frac{\underset{\rightarrow}{u}^*}{C_r^*} \quad , \quad p = \frac{p^*}{p_r^*}$$

$$s = \frac{s^*}{C_v^*} \quad , \quad \underset{\rightarrow}{\nabla} = L_r^* \underset{\rightarrow}{\nabla}^* \quad , \quad Q = \frac{Q^* R^* L_r^*}{P_r^* C_v^* C_r^*} \tag{B-5}$$

Since mass addition has been neglected, the above equations describe a constant composition flow whose behavior is controlled by external heat addition.

In the presence of small disturbances, the various quantities which appear in equations (B-1) through (B-4) can be expressed in the following form:

$$\rho = \bar{\rho} + \rho' \quad , \quad s = \bar{s} + s' \quad , \quad \underset{\rightarrow}{u} = \underset{\rightarrow}{\bar{u}} + \underset{\rightarrow}{u}'$$

$$p = \bar{p} + p' \quad , \quad Q = \bar{Q} + Q' \tag{B-6}$$

where barred quantities represent steady state quantities and the primed quantities represent time-dependent perturbations from the steady-state conditions. While the steady-state quantities are assumed to vary with axial direction (i.e., z), only the perturbations are allowed to depend on both time and three space directions. As is customary in stability analyses, the behavior of the steady-state flow must be obtained prior to the analysis of the behavior of the perturbations.

Substituting the expressions given in equation (B-6) into equations (B-1) through (B-4) and separating the latter into time-independent and time-dependent equations yields the following set of steady-state equations:

$$\bar{\rho} \frac{d\bar{u}}{dz} + \bar{u} \frac{d\bar{\rho}}{dz} = 0$$

$$\bar{u} \frac{d\bar{u}}{dz} + \frac{1}{\gamma \bar{p}} \frac{d\bar{p}}{dz} = 0$$

$$\frac{-\gamma \bar{p}}{\bar{\rho}} \bar{u} \frac{d\bar{\rho}}{dz} + \bar{u} \frac{d\bar{p}}{dz} = \bar{Q}(z) \tag{B-7}$$

$$\frac{d\bar{s}}{dz} = \frac{1}{\bar{p}} \frac{d\bar{p}}{dz} - \frac{\gamma}{\bar{\rho}} \frac{d\bar{\rho}}{dz}$$

Once $\bar{Q}(z)$, which represents the z dependence of the external heat addition, has been specified, the above equations can be solved to yield the axial variation of the various steady-state quantities.

Neglecting products of perturbations, using some of the steady-state equations, and recalling that the mean flow is irrotational, the conservation equations for the perturbations may be expressed in the following form:

$$\frac{\partial \rho'}{\partial t} + \nabla\cdot(\bar{\rho}\,\underset{\rightarrow}{u}' + \rho'\,\bar{u}) = 0 \tag{B-8}$$

$$\frac{\partial \underset{\rightarrow}{u}'}{\partial t} + \nabla(\underset{\rightarrow}{\bar{u}}\cdot\underset{\rightarrow}{u}') + (\nabla\times\underset{\rightarrow}{u}')\times\underset{\rightarrow}{\bar{u}} + \underset{\rightarrow}{\nabla}\left(\frac{p'}{\gamma\bar{\rho}}\right) - \frac{\nabla\bar{s}}{\gamma}\left(\frac{p'}{\gamma\bar{\rho}}\right) - \frac{\nabla\bar{u}^2}{2\gamma}s' = 0 \tag{B-9}$$

$$\frac{\partial s'}{\partial t} + (\underset{\rightarrow}{\bar{u}}\cdot\underset{\rightarrow}{\nabla})s' + (\underset{\rightarrow}{u}'\cdot\underset{\rightarrow}{\nabla})\bar{s} = \frac{Q'}{\bar{p}} - \frac{\bar{Q}p'}{\bar{p}^2} \tag{B-10}$$

$$s' = \left(\frac{\gamma\bar{\rho}}{\bar{p}}\right)\frac{p'}{\gamma\bar{\rho}} - \gamma\frac{\rho'}{\bar{\rho}} \tag{B-11}$$

Due to the cylindrical geometry of the combustor, a cylindrical coordinate system will be used in the analysis of the above equations. Expressed in a cylindrical coordinate system, equations (B-8) through (B-10) become:*

$$\frac{\partial \tau}{\partial t} + \frac{1}{\gamma}\frac{\partial}{\partial \tau}(\gamma v) + \frac{1}{r^2}\frac{\partial}{\partial \theta}(\zeta) + \frac{1}{\bar{\rho}}\frac{\partial}{\partial z}(\bar{\rho}u) + \frac{1}{\bar{\rho}}\frac{\partial}{\partial z}(\bar{\rho}\bar{u}\tau) = 0 \tag{B-12}$$

$$\frac{\partial u}{\partial t} + \frac{\partial}{\partial z}(\bar{u}u) + \frac{\partial \pi}{\partial z} - \frac{1}{\gamma}\frac{\partial \bar{s}}{dz}\pi - \frac{1}{2\gamma}\frac{d\bar{u}^2}{dz}s = 0 \tag{B-13}$$

$$\frac{\partial v}{\partial t} + \bar{u}\frac{\partial v}{\partial z} + \frac{\partial \pi}{\partial r} = 0 \tag{B-14}$$

$$\frac{\partial \zeta}{\partial t} + \bar{u}\frac{\partial \zeta}{\partial z} + \frac{\partial \pi}{\partial \theta} = 0 \tag{B-15}$$

where

$$\frac{\partial s'}{\partial t} + \bar{u}\frac{\partial s}{\partial z} + u\frac{ds}{dz} - \frac{1}{\bar{p}}\left(Q' - \frac{\bar{Q}\gamma\bar{\rho}}{\bar{p}}\pi\right) = 0 \tag{B-16}$$

$$\tau = \frac{\rho'}{\bar{\rho}} \quad ; \quad \pi = \frac{p'}{\gamma\bar{\rho}} \quad ; \quad \zeta = rw \tag{B-17}$$

and u, v and w respectively represent the axial, radial, and tangential components of the velocity perturbation.

*Whenever possible, the use of primes will be omitted from the remainder of the analysis.

Appendix

In a search for a solution of equations (B-12) through (B-16), it is assumed that the solutions to these equations can be expressed in the following form:

$$\begin{aligned} s &= S(z)\ K(r,\theta,t) \\ \tau &= R(z)\ K(r,\theta,t) \\ \pi &= P(z)\ K(r,\theta,t) \\ u &= U(z)\ K(r,\theta,t) \\ v &= V(z)\ K_r(r,\theta,t) \\ \zeta &= W(z)\ K_\theta(r,\theta,t) \end{aligned} \tag{B-18}$$

where

$$K = \Theta(\theta)\overline{\Psi}(r)e^{i\alpha t} \tag{B-19}$$

and

$$\alpha = \omega + i\lambda \tag{B-20}$$

Substituting the expressions given in equations (B-18) and (B-19) into equations (B-12) through (B-16) and separating variables yields the following system of differential equations:

$$i\alpha\overline{\rho}R + (\overline{\rho}U)' + (\overline{\rho}\,\overline{u}R)' = -\overline{\rho}\left\{V(z)\frac{(r\psi(r))'}{r\psi(r)} + W(z)\frac{\ddot{\Theta}(\theta)}{r^2\Theta(\theta)}\right\} \tag{B-21}$$

$$i\alpha U + (\overline{u}U)' + P' - \frac{1}{\gamma}\frac{d\overline{s}}{dz}P - \frac{1}{\gamma}\overline{u}\frac{d\overline{u}}{dz}S \tag{B-22}$$

$$i\alpha V + \overline{u}V' + P = 0 \tag{B-23}$$

$$i\alpha W + \overline{u}W' + P = 0 \tag{B-24}$$

$$i\alpha S + \overline{u}S' + \frac{d\overline{s}}{dz}U = \frac{Q'/K(r,\theta,t)}{\overline{p}} - \frac{\overline{Q}\gamma\overline{\rho}}{\overline{p}^2}P \tag{B-25}$$

$$S = \frac{\gamma\overline{\rho}}{\overline{p}}P - \gamma R \tag{B-26}$$

As can be seen by inspection of the above equations, complete separation of variables can be achieved only after Q' has been specified and only if:

$$W(z) = V(z) \tag{B-27}$$

Subtracting equation (B-24) from (B-23) and solving the resulting differential equation yields:

$$V(z) - W(z) = C_o f_o \tag{B-28}$$

where

$$C_o = W(z=0) - V(z=0) \tag{B-29}$$

and

$$f_o = \exp\left\{ \int_0^z \frac{i\alpha}{\bar{u}(z')}\, dz' \right\} \tag{B-30}$$

It thus follows that $V(z) = W(z)$ when C_o is identically zero. Assuming that $V(z)=W(z)$ and separating variables, equation (B-21) yields the following relations:

$$\Theta'' + n^2\Theta = 0 \tag{B-31}$$

$$r^2\psi'' + r\psi' + (S^2r^2 - n^2)\psi = 0 \tag{B-32}$$

$$i\alpha\bar{\rho}R + (\bar{\rho}U)' + (\bar{\rho}\bar{u}R)' - S^2\bar{\rho}V = 0 \tag{B-33}$$

Equation (B-31) describes the behavior of an harmonic oscillator, and its solution can be written as follows:

$$\Theta(\theta) = \begin{Bmatrix} \cos n\,\theta \\ \sin n\,\theta \end{Bmatrix} \qquad \text{for standing transverse modes}$$

or (B-34)

$$\Theta(\theta) = e^{\pm in\theta} \qquad \text{for traveling transverse modes}$$

Appendix

Equation (B-32) is the well-known Bessel differential equation whose solution for an annulus can be expressed as follows:

$$\psi(r) = \left\{ J_n(S^\sigma(n,q)r) + B^\sigma(n,q)\, Y_n^\sigma(S^\sigma(n,q)r) \right\} \tag{B-35}$$

Assuming that the combustor has a hard wall, then it can be shown (see Appendix B of reference 7) that the constants $B^\sigma(n,q)$ and $S^\sigma(n,q)$ are determined by the solution of the following two transcendental equations:

$$J_n'(S^\sigma(n,q)) + B^\sigma(n,q)\, Y_n'(S^\sigma(n,q)) = 0 \tag{B-36}$$

$$J_n'(\sigma S^\sigma(n,q)) + B^\sigma(n,q)\, Y_n'(\sigma S^\sigma(n,q)) = 0$$

where

$$\sigma = R_1/R_2 \tag{B-37}$$

To complete separation of variables in equation (B-25), it will be assumed that

$$Q' = Y\, Q(z)\, \pi \tag{B-38}$$

where Y is a complex number which relates the energy release perturbation to the pressure (i.e., π) perturbation. The fact that Y is a complex number implies that there is a phase as well as an amplitude relationship between the energy and pressure perturbations. Equation (B-38) implies that energy release responds primarily to pressure disturbances. The factor $\bar{Q}(z)$ which is included in equation (B-38) implies that the energy release perturbation is also dependent on the amount of "unused" chemical energy still available at location z; and Q' must equal zero when $\bar{Q}(z)$ is zero.

Integrating equations (B-23) and (B-25) to solve for $V(z)$ and $S(z)$, and using equation (B-26) to obtain an expression for $R(z)$ yields the following results:

$$V(z) = \left\{ V_o \int_0^z P \frac{f_o}{\bar{u}}\, dz \right\} \Big/ f_o(z) \tag{B-39}$$

$$R(z) = \left(\frac{\bar{\rho}}{\bar{p}}\right)P - \left\{ \left(\frac{\gamma\rho_o}{\bar{p}_o} P_o - \gamma R_o\right) + \int_0^z \left(\frac{Y\bar{Q}_o(z)}{\bar{p}}P - \frac{\bar{Q}_o\gamma\bar{\rho}}{\bar{p}}P - \frac{d\bar{s}}{dz}U\right)\frac{f_o}{\bar{u}}\, dz \Big/ \gamma f_o \right\} \tag{B-40}$$

where the subscript zero (i.e., $(\,)_o$ denotes quantities evaluated at $z = 0$.

Substituting the expressions for V(z) and R(z) (and derivatives) into equations (B-22) and (B-33) yields the following differential equations which control the behavior of U and P:

$$\bar{\rho}\bar{u}f_o P' + \left\{i\alpha\bar{\rho}f_o + \bar{\rho}\bar{u}\left(\frac{\bar{\rho}}{\bar{u}}\right)' f_o + \bar{u}\bar{\rho}\bar{Q} - \frac{1}{\gamma}\bar{u}\bar{\rho}Y\right\}P + S^{\sigma 2}(n,q)\int_0^z P\frac{f_o}{\bar{u}}\,dz'$$
$$+ \bar{P}f_o U' + \left\{\frac{1}{\gamma}\bar{\rho}\bar{u}\frac{d\bar{s}}{dz} + \bar{\rho}\left(\frac{\bar{\rho}}{\bar{u}}\right)f_o\right\}U - S^{\sigma 2}(n,q)\,V_o\,\bar{\rho} = 0 \qquad \text{(B-41)}$$

$$\gamma\bar{u}f_o U' + \left\{i\alpha f_o\gamma + \gamma f_o\bar{u}'\right\}U + \gamma f_o p' - f_o\frac{d\bar{s}}{dz}P + \bar{u}\bar{u}'\left\{S_o + \int_0^z\left(\frac{Y\bar{Q}(z)P}{\bar{\rho}}\right.\right.$$
$$\left.\left. - \frac{\bar{Q}\gamma\bar{\rho}}{\bar{\rho}}P + \frac{d\bar{s}}{dz}U\right)\frac{f_o}{\bar{u}}\,dz'\right\} = 0 \qquad \text{(B-42)}$$

It is possible to proceed with elimination of variables by integrating equation (B-41) to obtain an expression for U as a function of P and then substituting the resulting expression for U into equation (B-42). The resulting integro-differential equation for P can be shown to be equivalent to a fourth-order ordinary differential equation whose solution requires at least four boundary conditions to be imposed at the entrance and exit of the combustor.

Obtaining solutions to the resulting fourth-order differential equation for P is equivalent to solving equations (B-41) and (B-42) or to the solution of the system of equations composed of equations (B-22), (B-23), (B-25), (B-26), and (B-33). Inspection of these various equations reveals that some of their coefficients depend on the complex parameters α and Y whose determination will require the imposition of additional conditions upon the solutions of the differential equations.

Axial Boundary Conditions

It is the objective of this analysis to determine the dependence of the neutral stability limits of the combustor under consideration upon various design parameters. With this in mind, it is convenient to let $\lambda = 0$ specify the value of $\alpha = \omega$ and then attempt to determine the complex constant Y by imposing appropriate boundary conditions.

The boundary conditions at the entrance and exit of the combustor are respectively determined by the behavior of the pressure oscillations in the diffuser and in the annular air jet that leaves the combustor. Since neither of these problems has yet been solved, it becomes necessary to derive an approximate set of boundary conditions.

In the present study, the flow enters the combustor through a series of screens whose main task is to assure the uniformity of the entering flow. Denoting the location of the screens by $z = 0$, assuming that the flow passing through the screen is uniform and axial, and recalling that there is no combustion at the screens, it is possible to impose the following approximate boundary conditions:

$$V_o = S_o = 0 \qquad \text{(B-43)}$$

On physical grouns, it is possible to argue that in the immediate vicinity of the screens,

the flow is quasi-steady (i.e., $\partial/\partial z \gg \partial/\partial t$). Under these conditions, it is possible to state that the Mach number of the entering flow is constant; that is

$$\frac{\bar{u} + u'}{\bar{C} + C'} = M_o = \text{CONSTANT} \tag{B-44}$$

It follows from equations (B-43) and (B-44) that at

$$U_o = M_o \left(\frac{\gamma - 1}{2\gamma}\right) \bar{P}_o^{-(\gamma+1/2\gamma)} P_o \tag{B-45}$$

The fourth boundary condition is obtained by specifying P_o. There is no loss of generality if

$$P_o = 1 \tag{B-46}$$

The fifth boundary condition should be specified at the combustor exit. Since the pressure oscillations in the combustor are neutrally stable, over a period of an oscillation there can be no net accumulation of mass in the combustor. This condition can be expressed as follows:

$$< \int_{c.s.} (\bar{\rho}\underset{\rightarrow}{u}' + \rho'\underset{\rightarrow}{u}' + \rho'\bar{u}) \cdot \underset{\rightarrow}{n}\, ds > = 0 \tag{B-47}$$

where the brackets < > represent time averaging over a period of the oscillation and the integration is performed over the control surface of the combustor. Performing the above integration and using equation (B-44) yields the following boundary condition that must be satisfied at

$$\sqrt{U_r(L)^2 + U_i(L)^2}\ \sqrt{R_r(L)^2 + R_i(L)^2}\ \cos\left\{\tan^{-1}\frac{R_i(L)}{R_L(L)} - \tan^{-1}\frac{U_i(L)}{U_R(L)}\right\} = M_o \frac{\gamma-1}{2\gamma} \bar{P}_o^{-(\gamma+1/2\gamma)} \tag{B-48}$$

Method of Solution

In most stability studies, it is customary to specify the complex number Y, which describes the unsteady combustion process, and then to solve for the complex eigenvalue α that describes the frequency and growth (or decay) rate of the oscillations. Due to our inability to describe the combustion process adequately, an inverse approach has been chosen. In this case α is specified apriori, and the complex constant Y is determined by requiring the various solutions to satisfy the imposed boundary conditions.

Using such an approach, it will be possible to determine, for a given combustor design and given operating conditions, the values of Y (corresponding to different values of $\alpha = i\omega$) for which the operation of the combustor is neutrally stable. The curve formed by the calculated values of Y will divide the complex Y plane into linearly stable and linearly unstable regions. Stability characteristics of the afterburner can be determined by comparing Y -plots which were obtained for various combustors. If a given design change resulted in an increase of the unstable region of operation (in the Y plane), it may be concluded that such a design change may result in a more unstable combustor.

In the present study, it was decided to determine Y by numerically solving equations (B-7), (B-22), (B-23), (B-25), (B-26), and (B-33). To proceed with the numerical solution, it is necessary to specify $\bar{Q}(z)$, the steady-state heat addition, ω, $B^{\sigma}(m,q)$, $S^{\sigma}(m,q)$, α and γ. Once these quantities are available, a value of Y is guessed, and the numerical integration starts at $z = 0$ by satisfying the conditions specified in equations (B-43) through (B-44). The numerical solution proceeds to $z = L$ where the boundary condition given by equation (B-46) must be satisfied. If the numerically calculated solutions fail to satisfy this boundary condition, a new value of Y is guessed, and the numerical integration is repeated. This procedure is repeated until a value of Y that "enables" the numerical solutions to satisfy all the boundary conditions is chosen. Additional values of Y are then determined by changing the value of ω.

It is the objective of this computer study to determine the effect that changes in steady-state combustion distribution and combustor geometry have on the stability of the annular afterburner.

Figure 32 is a stability curve that was calculated for the 1,0 mode for a combustor with hub tip ratio of 0.5 and assuming the energy release distribution shown in figure 33. The energy release distribution was assumed uniform over each cross-section normal to the z axis. The values for various parameters chosen are typical of a combustor that might be tested if the concepts of this report are pursued further.

Ordinarily, the energy release distribution and geometry of the combustor under study would be varied and the resulting stability plots compared to ascertain the effects of these factors on high-frequency combustion instability. However, there was only time enough available during the course of this contract to generate one curve as a test of the computer program. Also, as there was not sufficient time to determine which region is stable and which is unstable, only the stability boundary is shown in figure 32.

For several reasons, points on the curve shown were rather difficult to obtain. In searching for the eigenvalues, it is necessary to find minimums or valleys in a three-dimensional surface. The surface is relatively flat except in a small neighborhood about the minimum, where there is a deep pit with steep walls. This condition, combined with the fact that the search procedure was far from optimum, made location of eigenvalues rather difficult. However, this difficulty may soon be largely alleviated as a result of work being done on a similar problem, concerned with duct acoustics, the results of which can readily be adapted to the solution of this problem.

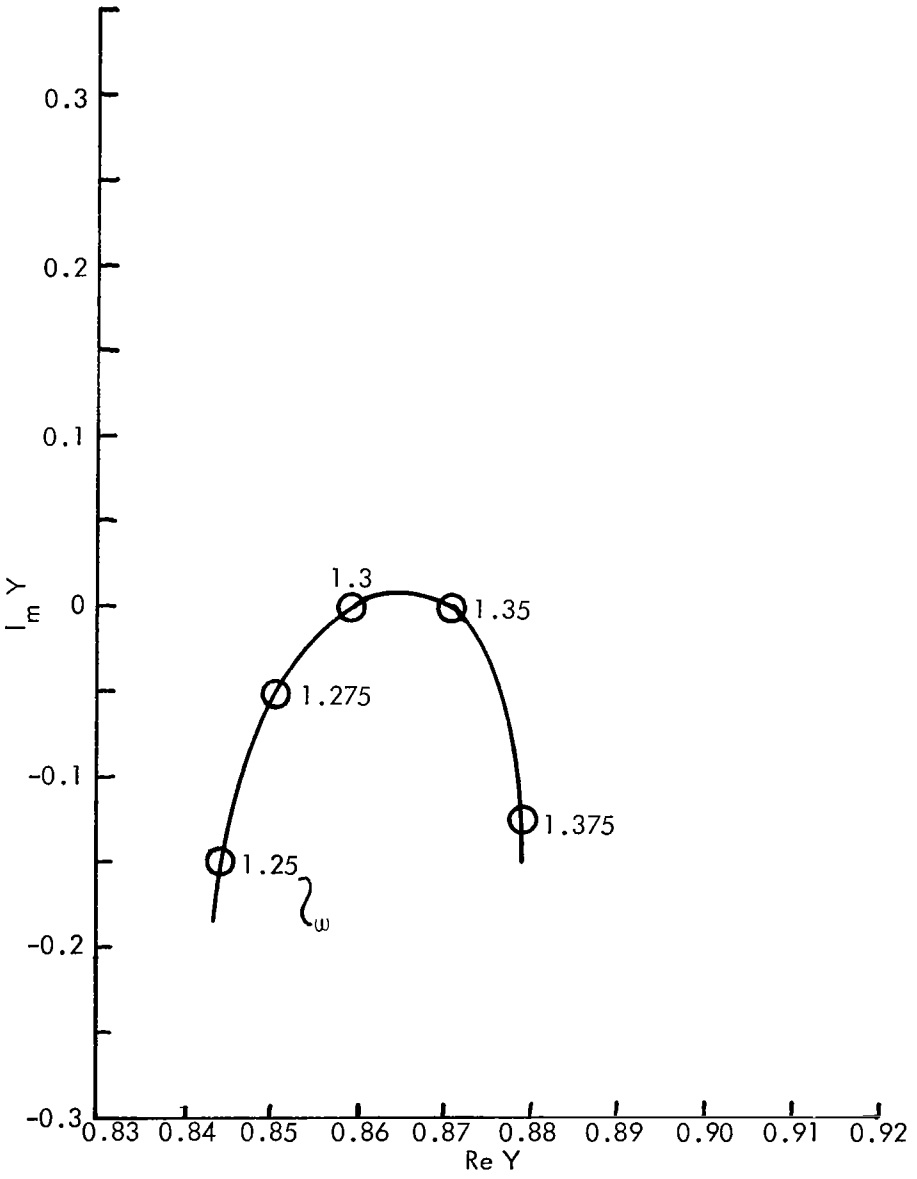

FIGURE 32 STABILITY BOUNDARY FOR TYPICAL COMBUSTOR

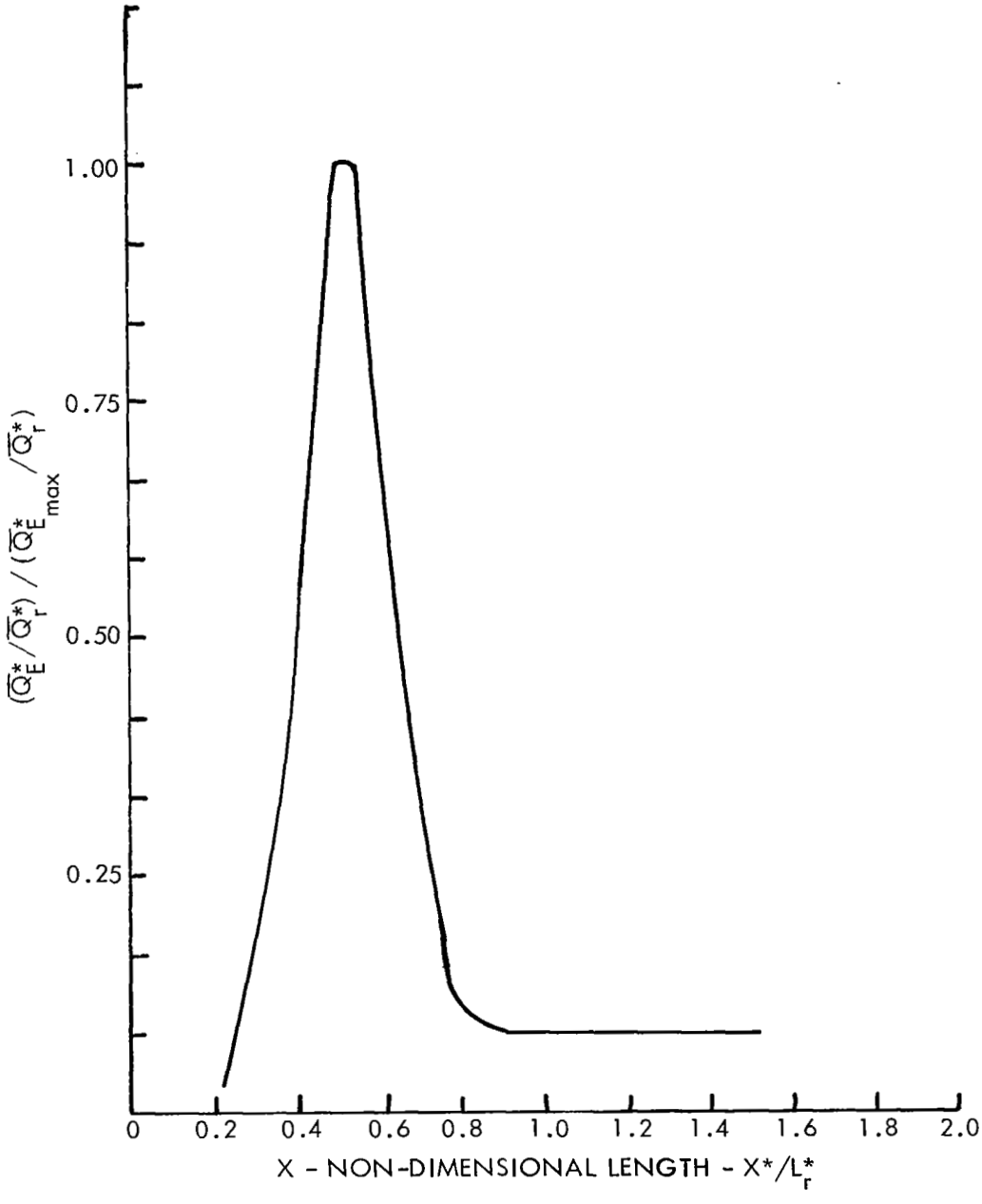

FIGURE 33 ENERGY RELEASE DISTRIBUTION AS A FUNCTION OF AXIAL DISTANCE

REFERENCES

1. Haddle, G. P.; and Plumblee, H. E.: Jet Noise Tests to Determine Effects of Exhaust Gas Heating. Paper presented at 76th Meeting of Acoustical Society of America (Cleveland, Ohio), Nov. 1968.

2. Haddle, G. P.; Wynne, G. A.; and Mathis, J. T.: Tests to Determine the Relationship Between Jet Exhaust Temperature and Radiated Jet Noise. ER-9571, Aerospace Sciences Lab., Lockheed-Georgia Company, March 1969.

3. Lassiter, Leslie W.; and Hubbard, Harvey H.: Experimental Studies of Noise from Subsonic Jets in Still Air. NACA TN 2757, 1952.

4. Plumblee, H. E.; Ballentine, J. R.; and Passinos, B.: Near Field Noise of Aircraft Propulsion Systems with Emphasis on Prediction Techniques for Jets. AFFDL-TR-67-43, 1967.

5. Doak, P. E.: Ch II, Elements of Sound Propagation Noise and Acoustic Fatigue in Aeronautics. Richards, E. J.; and Mead, D. J.; eds., John Wiley and Sons, Ltd., 1968.

6. Mungur, P.; and Plumblee, H. E.: The Propagation and Attenuation of Sound in a Soft-Walled Annular Duct Containing Sheared Flow. Proceedings of NASA Basic Noise Conference, July 14-15, 1969, Washington, D.C.

7. Tyler, J. M.; and Sofrin, T. G.: Axial Flow Compressor Noise Studies. SAE Transactions, vol. 70, 1962, pp. 309.

8. Anon.: FAA Noise Notice of Public Rulemaking. 69-1, Jan. 3, 1969.

9. Kramer, James J.: Quiet Engine Program-Detailed Engine Designs. Proceedings of the NASA-Langley Conference on Progress of NASA Research Relating to Noise Alleviation of Large Subsonic Jet Aircraft, NASA SP-189, 1968, pp 263-272.

10. Anon.: DC-8 Noise Reduction Tests Successfully Completed. Aerospace Daily, March 21, 1969, P. 88.

11. Spalding, D. B.: The Spread of Turbulent Flames Confined in Ducts. Eleventh Combustion Symposium, 1966.

12. Prince, W. R.; Velie, W. W.; and Braithwaite, M.: Full-Scale Evaluation of Some Flameholder Design Concepts for High-Inlet-Velocity Afterburners. NACA RM E56D10, June, 1956.

13. Schubauer, G. B.; and Spangenberg, W. G.: Effect of Screens in Wide-Angle Diffusers. Report 949, National Bureau of Standards, 1947.

14. Annand, W. J. D.: The Resistance of Air Flow of Wire Gauges. J. Roy. Aeron. Soc., March 1953.

15. Longwell, J. P.: Combustion of Liquid Fuels. High Speed Aerodynamics and Jet Propulsion, Volume II, Part IV, Sect. J, Lewis, B; et al, ed., Princeton University Press, 1959, pp 407-443.

16. Ilyashenko, S. M.; et al: Theory and Analysis of Straight-Through-Flow Combustion Chambers. FTD-MT-65-143, Foreign Technology Division, Wright-Patterson AFB, Ohio, 1966.

17. Hazard, H. R.: A Review of Research on Spark Ignition. TR 15037-1, Battelle Memorial Institute, March 1952.

18. Lewis, B.; and Von Elbe, G.: Combustion Flames and Explosions. Academic Press, Inc., New York, N. Y., 1951.

19. Belles, Frank E.; and Swett, Clyde C.: Ignition and Flammability of Hydrocarbon Fuels. Basic Considerations in the Combustion of Hydrocarbon Fuels with Air. Barnett, Henry C.; and Hibbard, Robert R., eds., NACA TR 1300, 1957, pp 83-126.

20. Spalding, D. B.: Some Fundamentals of Combustion. Butterworths Scientific Publications, 1955.

21. Staff of Lewis Laboratory: A Summary of Preliminary Investigations into the Characteristics of Combustion Screech in Ducted Burners. NACA TR 1384, 1958.

22. Haddock, Gordon W.: Flame-Blowoff Studies of Cylindrical Flame Holders in Channeled Flow. J. P. L. Progress Report 3-24, Jet Propulsion Lab, 1951.

23. Hirschfelder, Joseph O.; Curtiss, Charles F.; and Bird, Byron F.: Molecular Theory of Gases and Liquids. John Wiley and Sons, Inc, New York, N. Y., 1964.

24. Hirschfelder, J. O.: Heat Transfer in Chemically Reacting Mixtures. J. Chem. Phys. Vol. 26, No 2, 1957.

25. Lees, L.: Convective Heat Transfer with Mass Addition and Chemical Reactions. Combustion and Propulsion Third AGARD Colloquim, Pergamon Press, New York, 1958, pp 451-498.